Development of Targetable Two-Photon Fluorescent Probes to Image Hypochlorous Acid in Mitochondria and Lysosome in Live Cell and Inflamed Mouse Model

Lin Yuan[1,2‡], Lu Wang[1‡], Bikram Keshari Agrawalla[1], Sung-Jin Park[3], Hai Zhu[1], Balasubramaniam Sivaraman[3], Juanjuan Peng[3], Qing-Hua Xu[1], Young-Tae Chang[1,3]*

[1]Department of Chemistry, National University of Singapore, Singapore 117543

[2]State Key Laboratory of Chemo/Biosensing and Chemometrics, College of Chemistry and Chemical Engineering, Hunan University, Changsha 410082, PR China

[3]Laboratory Bioimaging Probe Development, Singapore Bioimaging Consortium, Singapore 117543

ABSTRACT

Hypochlorous acid (HOCl), as a highly potent oxidant, is well known as a key "killer" for pathogens in innate immune system. Recently, mounting evidence indicates that intracellular HOCl plays additional important roles in regulating inflammation and cellular apoptosis. However, the organelle(s) involved in the distribution of HOCl remain unknown, causing difficulty to fully exploit its biological functions in cellular signaling pathways and various diseases. One of the main reasons lies in the lack of effective chemical tools to directly detect HOCl at sub-cellular levels due to low concentration, strong oxidization and short lifetime of HOCl. Herein, the first two-photon fluorescent HOCl probe (**TP-HOCl 1**) and its mitochondria- (**MITO-TP**) and lysosome- (**LYSO-TP**) targetable derivatives for imaging mitochondrial and lysosomal HOCl were reported. These probes exhibit fast response (within seconds), good selectivity and high sensitivity (< 20 nM) toward HOCl. In live cell experiments, both mitochondria- (**MITO-TP**) and lysosome- (**LYSO-TP**) targetable probes were successfully applied to detect intracellular HOCl in corresponding organelles. In particular, the two-photon imaging of **MITO-TP** and **LYSO-TP** in murine model shows that both higher amount of HOCl can be detected in lysosome and mitochondria of macrophage cells during inflammation condition. Thus, these probes could not only help clarify the distribution of sub-cellular HOCl, but also serve as excellent tools to exploit and elucidate functions of HOCl at sub-cellular levels.

Introduction

The study of reactive oxygen species (ROS) is attracting increasing attention due to their essential roles in cell signaling and homeostasis, such as aging,[1] pathogen response,[2] anti-inflammation regulation.[3] Among various ROS, hypochlorous acid (HOCl) as a highly potent oxidant generated during phagocytosis, seems to mainly serve as a "killer" for pathogens in innate immune system.[4] It is usually produced by myeloperoxidase (MPO)-catalyzed per-oxidation of chloride ions in phagolysosome, where pathogens are engulfed and decomposed[5] (Figure 1). In addition to phagosomal HOCl in the presence of pathogens, mounting evidence demonstrates that nonphagosomal intracellular HOCl (nphHOCl) generation can be induced by a variety of soluble stimuli,[6,7] which helps suppress inflammation and regulate cellular apoptosis.[8,9] Furthermore, it is reported that nphHOCl may also be implicated in neurodegenerative disorders[10] such as Parkinson's disease[11] and cerebral ischemia.[12] At the same time, HOCl could cause mitochondrial permeabilisation,[13] lysosomal rupture[14] and cell death through calcium dependent calpain activation.[13] However, the distribution of nphHOCl at sub-cellular levels is still unclear, which causes severe difficulty

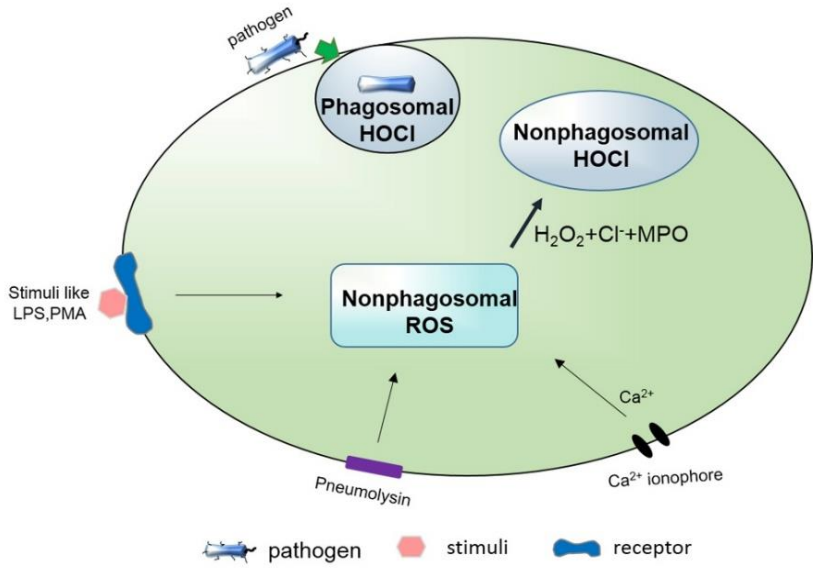

Figure 1. Stimuli that induce intracellular HOCl. Apart from ingested particles that give rise to phagosomal HOCl (phHOCl) production (left), certain stimuli, such as LPS, lead to nonphagosomal HOCl (nphROS) production without being ingested (right). H_2O_2, hydrogen peroxide; MPO, myeloperoxidase.

to fully exploit and elucidate intracellular functions of nphHOCl.[15] One of the main reasons lies in lack of efficient tools to directly real-time monitor nphHOCl at sub-cellular level due to its strong oxidization,[16] short-lived time[17] and relatively low concentration.[18] Therefore, it is challenging and highly desired to prepare novel chemical tools for elucidating the distribution and functions of nphHOCl at sub-cellular level.

Fluorescence imaging possesses unique advantages for the observation of functional and molecular recognition events in live cells.[19,20] Furthermore, it has emerged as the irreplaceable technique to monitor the level, localization, and movement of bio-molecules at sub-cellular levels.[21-25] Among various types of optical imaging techniques, two-photon microscopy (TPM) offers a high-resolution imaging, deep penetration and low photo-toxicity due to the remarkably focused excitation and reduced scattering of near-infrared light in biological tissues.[26-29] Recently, the detection of HOCl was implemented by some good probes with different recognition moieties, including dibenzoylhydrazine,[30] p-methoxyphenol,[31,32] oxime,[33-36] selenide,[37-40] thiol compounds (internal thioester[41-44], thioether[45,46,6,72] and thiosemicarbazide[48]) and other groups,[47,49,64] which were specified in Table S1. Even most of these probes have been successfully applied to image intracellular HOCl, few probes were used to real-time detect HOCl at *sub-cellular* levels. On the other hand, it was assumed that nphHOCl may be generated in both mitochondria and lysosome of macrophage cells due to the intracellular distribution of MPO that catalyzes HOCl production.[50,51] Nevertheless, to the best of our knowledge, except for several mitochondria-located fluorescent probes for the detection of intracellular HOCl,[46,52,73], there is no report yet describing a fluorescent probe for successful detection of intracellular HOCl in lysosome, even there were two reported lysosome targeting probes with exogenously added HOCl.[40,53] The aforementioned concerns encouraged us to develop novel two-photon fluorescent probes to sense this important biomolecule and clarify its distribution in live cell and inflamed mouse model.

Herein, we report the first two-photon fluorescent "turn-on" HOCl probe (**TP-HOCl 1**) and its mitochondria- (**MITO-TP**) and lysosome- (**LYSO-TP**) targetable derivatives, which can image intracellular HOCl in live cell and inflamed mouse model. In the presence of HOCl, **TP-HOCl 1** exhibits a dra-

matic fluorescence increase with very short response time (within seconds), excellent selectivity and high sensitivity (16.6 nM). Besides, in live cell experiments, it is clearly indicated that **MITO-TP** and **LYSO-TP** can respond towards HOCl in mitochondria and lysosome. Furthermore, these probes were successfully applied to image mitochondrial and lysosomal HOCl in inflamed mouse model through two-photon imaging.

RESULTS AND DISCUSSION

Design and synthesis of HOCl probes. Acedan, as a well-known two-photon fluorophore,[54-57] was chosen as the fluorescence reporting group due to its excellent photo-physical properties resulting from the typical "push-pull" (amine-ketone) structure (scheme 1A).[57] Thus, it is predictable that protection of the ketone will decrease the "pull" ability thereby quenching the fluorescence of Acedan. On the other hand, it is reported that thiol atom in methionine is easily oxidized in tandem to sulfoxide and sulphone by HOCl.[58] Thus, 2-mercaptoethanol and 1, 2-ethanedithiol were employed to protect the ketone of acedan in the design of HOCl probes (**TP-HOCl 1** and **TP-HOCl 2**). It was expected that both compounds will be non-fluorescent or weakly fluorescent due to the disruption of the "push-pull" structure; however, reaction with HOCl, which de-protects the oxathiolane/mercaptal group to reveal the ketone, would lead to fluorescence enhancement. This expectation was further supported by the significantly increased oscillator strength of **TP-HOCl 1** (f, from 0.067 to 0.44) before and after reacting with HOCl calculated by density functional theory (DFT) (Figure S1). For comparison, oxime, a known reaction site for HOCl,[33, 34, 36, 59] was also introduced by combining hydroxylamine with acedan (**TP-HOCl 3**). Through comparison of response ability of three probes to HOCl, **TP-HOCl 1** was chosen as ideal HOCl probe, which was specified in the following paragraphs.

To monitor HOCl at sub-cellular levels, lysosome- and mitochondria- targetable groups (morpholine[60] and triphenylphosphine[61]) were further introduced to ensure the probe's intracellular localization. In addition, to avoid affecting the sensitivity of the probe, these groups were carefully positioned at the

other end of acedan to generate long distance gap from the reaction site. The lysosomal HOCl probe **Lyso-TP** and mitochondrial HOCl probe **Mito-TP** were effectively prepared from cyclization reaction of precursor **4** or **7** with 2-mercaptoethanol (Scheme 1E). The precursor **4** was synthesized through the hydrolysis of commercially available dye 6-methoxy-2-acetonaphthone and subsequent amination of intermediate **3** with 4-(2-aminoethyl)morpholine. The precursor **7** was readily synthesized

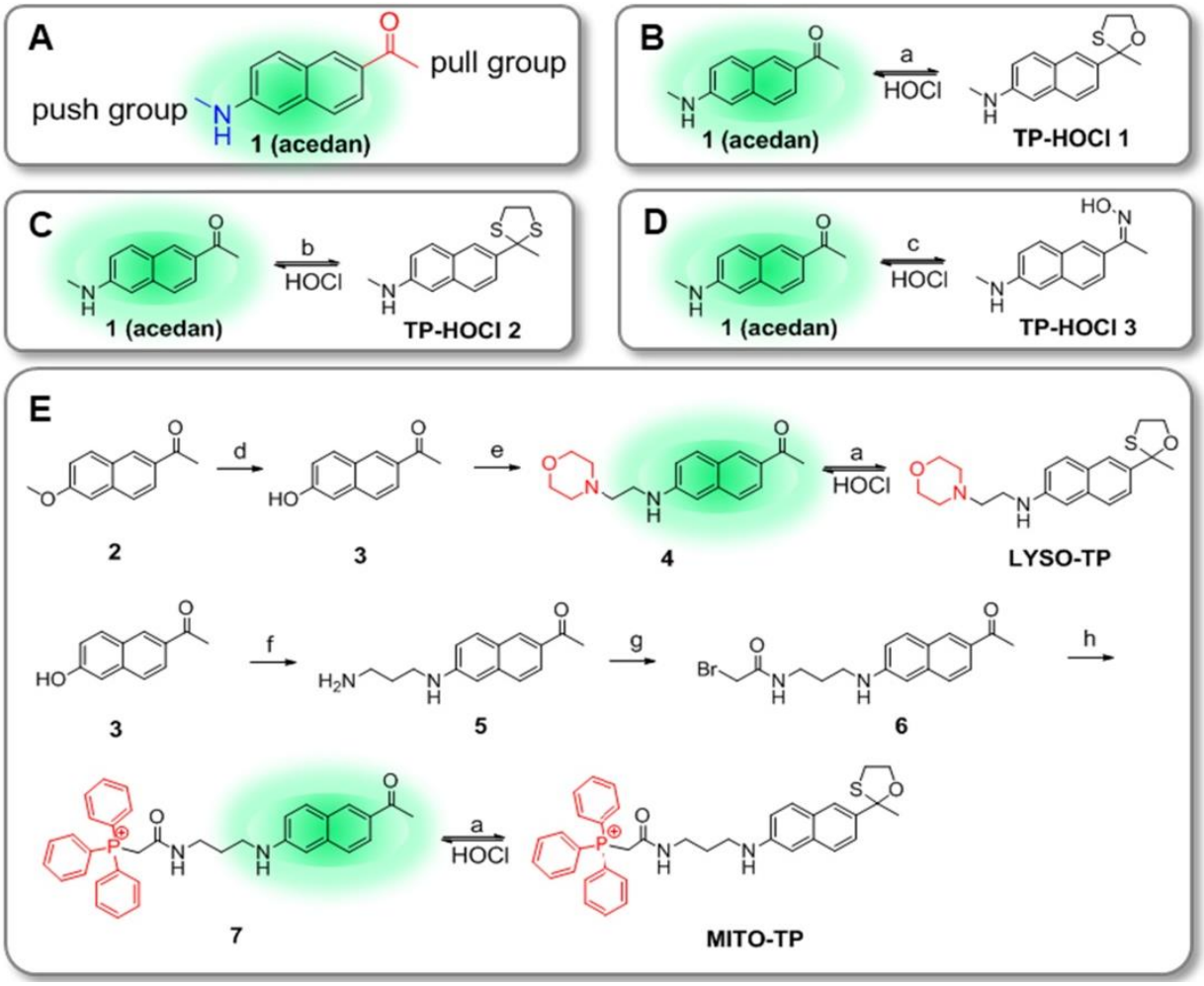

Scheme 1. The synthesis and proposed sensing mechanism of probes for HOCl. Reagents and conditions: a) 2-mercaptoethanol, 50 ˚C, 3 h. b) 1,2-ethanedithiol, 50 ˚C, 3 h. c) hydroxylamine, 50 ˚C, 3 h. d) 37% HCl, reflux, 48 h. e) 2-morpholinoethanamine, $Na_2S_2O_5$, microwave 80 W, 160 ˚C, 5 h. f) propane-1,3-diamine, $Na_2S_2O_5$, microwave 80 W, 160 ˚C, 6 h. g) 2-bromoacetyl chloride, r.t., 50 min. h) triphenylphosphine, r. t., 16 h.

through amination of intermediate **3** with 1, 3-propanediamine, and then amide coupling with 2-bromoacetyl chloride, and finally salt formation with triphenylphosphine. The detailed synthetic procedures, NMR and HRMS spectra were displayed in supporting information.

Comparing the fluorescent response of TP-HOCl 1-3 to HOCl. To compare the fluorescent response of **TP-HOCl 1-3** to HOCl, three probes were titrated with HOCl from 0 to 75 μM. Compared to **TP-HOCl 2**, the fluorescence intensity ratio (F/F_0 at 500 nm) of **TP-HOCl 1** was enhanced more significantly at low concentration of HOCl (Figure 2A) thereby indicating higher sensitivity. One reason may be due to the single sulfur atom in 1, 3-oxathiolane, which would require less HOCl for complete oxidization of **TP-HOCl 1**. Different from **TP-HOCl 1** and **TP-HOCl 2**, oxime-based probe **TP-HOCl 3** shows only slight response to HOCl, which may be attributed to the more effective oxidative de-protection of oxime by HOCl under basic condition.[33] Therefore, **TP-HOCl 1** was chosen as the probe for HOCl detection and its basic photo-physical properties were examined (Table S2 and Figure S2).

Fluorescent response of TP-HOCl 1 to HOCl. To investigate the sensitivity, selectivity and response time of **TP-HOCl 1** to HOCl, fluorescence spectroscopy was measured at various concentrations of HOCl. As it is shown in Figure 2B, the fluorescence intensity of **TP-HOCl 1** at 500 nm increased more than 670 fold when 20 equivalents of HOCl was added, which results from the recovery of "push-pull" structure of acedan when the oxathiolane was de-protected by HOCl. Moreover, **TP-HOCl 1** could respond to low concentration of HOCl with detection limit up to 16.6 nM (Figure S3), which indicates the high sensitivity of probe **TP-HOCl 1** to HOCl and the ability of probe **TP-HOCl 1** to monitor trace amounts of intracellular HOCl. In addition, the time dependent fluorescence intensity changes of probe **TP-HOCl 1** to HOCl revealed that the reaction can be completed within seconds at different pH buffer

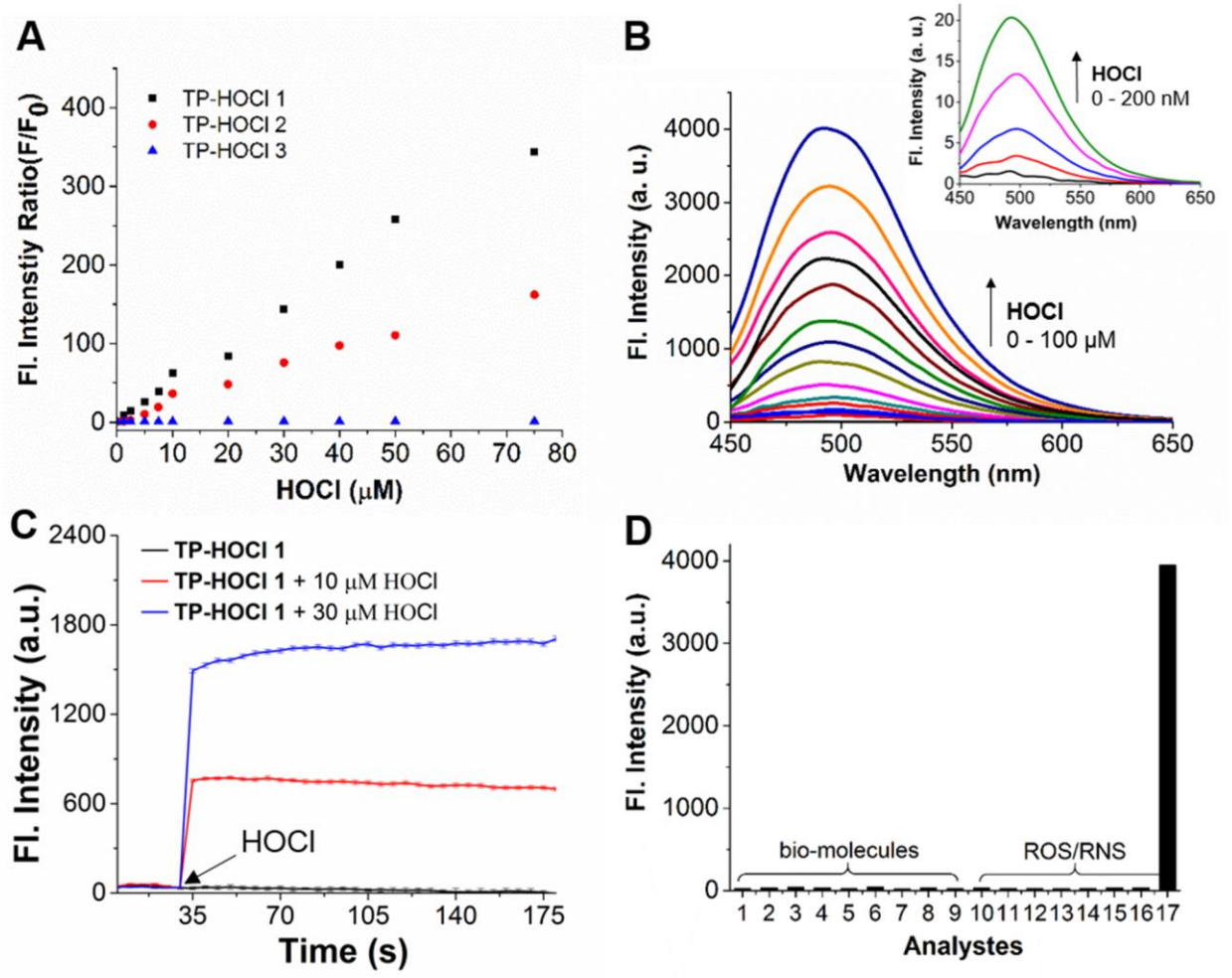

Figure 2. Fluorescence spectra of **TP-HOCl 1-3** responding to HOCl in PBS/EtOH (1:1, pH 7.4) solution. A) Plot of fluorescence intensity ratio (F/F_0 at 500 nm) changes of **TP-HOCl 1-3** as a function of HOCl concentrations, data acquired at 20 seconds after addition of HOCl (λ_{ex} = 375 nm). B) Fluorescence enhancement of **TP-HOCl 1** (5 μM) as a function of HOCl (0 to 100 μM). Inset shows Fluorescence spectra of **TP-HOCl 1** (0.5 μM) before and after adding HOCl at low concentrations (0 to 200 nM). C) The time course of fluorescence intensity of **TP-HOCl 1** before and after adding 10 μM and 30 μM of HOCl. D) Fluorescence responses of **TP-HOCl 1** (5 μM) towards various analytes (50 μM for biomolecules (1-9) and 100 μM for other ROS/RNS (10-17)). 1) PBS; 2) ATP; 3) ADP; 4) NAD; 5) GSH; 6) Cys; 7) Fe^{3+}; 8) Zn^{2+}; 9) Cu^{2+}; 10) H_2O_2; 11) •OH; 12) *t*-BuOOH; 13) *t*-BuOO•; 14) NO•; 15) O_2^-; 16) $ONOO^-$; 17) HOCl.

(pH 5.5, 7.4, 9.2) and the fluorescent signals remained nearly unchanged over time (Figure 2C and S4), which enables its real-time detection of HOCl. However, no fluorescence change was observed when **TP-HOCl 1** was incubated with other ROS (50 μM) and bio-molecules (100 μM) (Figure 2D). In addition, selectivity (HOCl 50 μM and other ROS 250 μM) was further examined at pH 5.5 and 7.8, which were chosen to mimic the lysosomal and mitochondrial pH respectively. As shown in Figure S5, **TP-HOCl 1** can also respond to HOCl rather than other ROS in both weak acid and basic environment. Notably, H_2O_2, a precursor of HOCl, does not interfere with the detection of HOCl even at 500 μM (Figure S6). In addition, **TP-HOCl 1** displayed almost no response to another highly potent oxidant, peroxynitrite ($ONOO^-$) (Figure S7), in good agreement with previous reported probes with thioester[41-44] and thioether[45,46,6,39] as recognition moieties. **TP-HOCl 1** is thus a good HOCl probe with high sensitivity, remarkable selectivity and very short response time.

Effect of pH to response ability and stability of TP-HOCl 1. To test the feasibility of **TP-HOCl 1** as HOCl probe, the performance of **TP-HOCl 1** to HOCl in PBS buffers with different pH values ranging from 4 to 9 was tested. As shown in Figure S8, after addition of HOCl, remarkable fluorescence enhancement of **TP-HOCl 1** could be observed immediately at wide pH ranges (pH 4 to 9) without significant variances, indicating that the assay is compatible with most intracellular pH environments. Even it was reported that pH may affect the oxidizing rate of hypochlorite,[62] it was difficult to discriminate the difference under various pH conditions because of the fast response of thioehter to hypochlorite, which can be achieved within seconds. Similar results can also be observed in the previous thioether-based probes.[45,63] Meanwhile, a stability test for **TP-HOCl 1** in PBS buffer was also conducted to check whether the oxathiolane group of **TP-HOCl 1** is stable at intracellular pH values (pH 4 to 9). As indicated by Figure 3A, almost no fluorescence changes were observed even after 4 hour incubation, while strong fluorescence was recovered after addition of 40 μM HOCl, which suggests the stability of **TP-HOCl 1**. Therefore, these results clearly demonstrate the feasibility of **TP-HOCl 1** responding towards HOCl in a broad range of pHs.

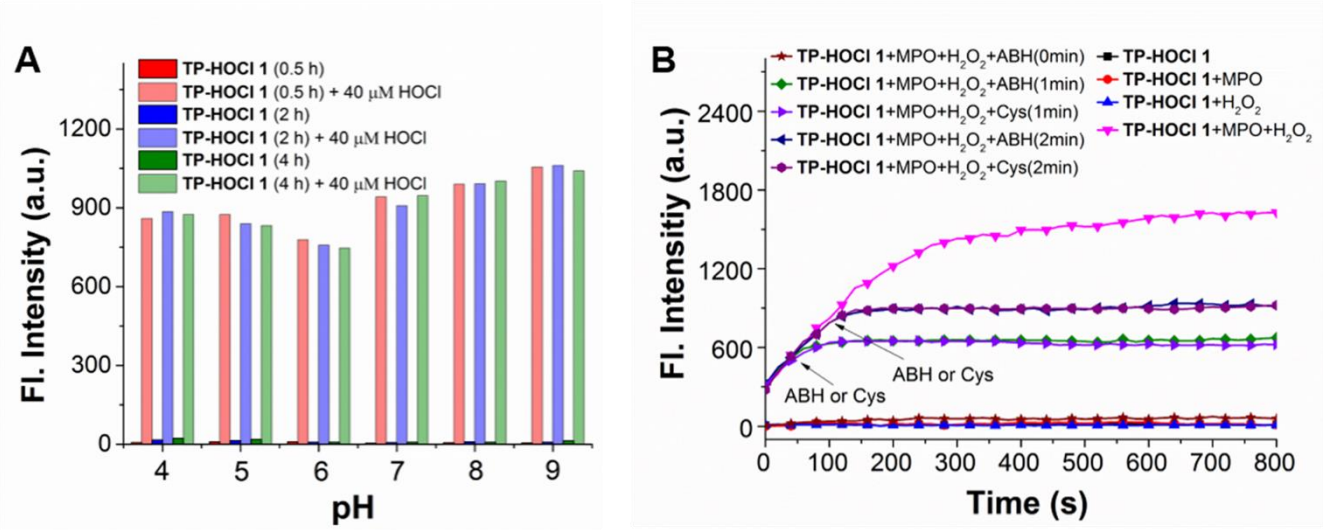

Figure 3. A) Probe **TP-HOCl 1** (5 μM) could kept stable in physiological pHs (pH 4-8). Probe was incubated in various pH buffers (pH 4-9) for 0.5, 2, 4 h respectively, and then 40 μM HOCl was added. B) Fluorescence responses of **TP-HOCl 1** towards HOCl generated in MPO/H_2O_2/Cl^- system (PBS, 20 μM H_2O_2, 1 U/mL MPO, pH=7.4, 37 ˚C). ABH (4-Aminobenzoic acid hydrazide, 10 μM) or Cys (cysteine, 200 μM) was added at 1 and 2 min respectively. MPO: Myeloperoxidase; ABH: MPO inhibitor.

Fluorescent response of TP-HOCl 1 to HOCl generated in Myeloperoxidase (MPO)/H_2O_2/Cl^- system. With the favorable features of **TP-HOCl 1** demonstrated, the feasibility of real-time detection of HOCl generation in an enzyme system was further investigated. MPO/H_2O_2/Cl^- system (PBS, 20 μM H_2O_2, 1 U/mL MPO, pH=7.4, 37 ˚C) was used to mimic the generation of HOCl inside cells. As shown in Figure 3B, the fluorescence intensity of **TP-HOCl 1** was increased immediately after addition into MPO/H_2O_2/Cl^- system. Continuous fluorescence increase over time was observed (within 15 min) due to gradual production of HOCl. Nevertheless, almost no variation in the fluorescent signals was observed in the presence of only MPO or H_2O_2, which demonstrated that HOCl rather than H_2O_2 or MPO is the target analyte. Furthermore, there is no obvious signal increase after inhibition of MPO by addition of 4-aminobenzoic acid (ABH, an MPO inhibitor) into the MPO/H_2O_2/Cl^- system. Importantly, after addition of ABH or cysteine at 1 and 2 min, the increasing fluorescence intensity was inhibited immediately thereby showing plane lines. Taken all together, **TP-HOCl 1** was successfully used in real-time

detection of HOCl generation in MPO/H_2O_2/Cl^- system, enabling itself to be a promising probe for studying HOCl-related biological processes.

Mechanism of TP-HOCl 1 responding to HOCl. To further examine the sensing mechanism of probe **TP-HOCl 1**, reversed-phased HPLC-MS was used to clarify the process of the reaction between **TP-HOCl 1** and HOCl. The HPLC chromatograms of **TP-HOCl 1** and compound **1** were shown in Figure S9A and D. After incubation with HOCl (100 μM and 200 μM) for 1 min (Figure S9C, D), except the peaks from **TP-HOCl 1** and de-protected compound **1**, a new peak with longer retention time was observed. This compound was purified and identified as the chlorinated product (compound **9**) through ^{1}H NMR, ^{13}C NMR and HRMS (Figure S10A-C). Meanwhile, the position of chlorine atom was further verified by H-H COSY, indicating that chlorine atom locates at C-7 rather than C-5 (Figure S10D). A similar chlorination reaction with HOCl was also observed in other fluorophores, such as Si-fluorescein and rhodamine.[43,64] In particular, the photo-properties of compound **9,** such as quantum yield and two-photon cross section, were measured, which suggests comparability with that of compound **1** (Table S2) thereby demonstrating little interference for further experiment. Taken together, a possible sensing mechanism of probe **TP-HOCl 1** to HOCl is proposed and shown in Figure 4. Non-fluorescent **TP-HOCl 1** is initially oxidized by HOCl to intermediate sulfoxide compound **8**, further oxidized to unstable sulphone and finally hydrolyzed to generate fluorescent compound **1**. Then compound **1** was partially chlorinated to compound **9** by excessive HOCl. In addition, to verify the above sensing mechanism, intermediate sulfoxide compound **8** was also prepared. Notably, compared with **TP-HOCl 1**, unstable compound **8** is more easily oxidized to compound **1** by HOCl (Figure S11), suggesting that sulfoxide compound **8** is the possible intermediate of the oxidation process.

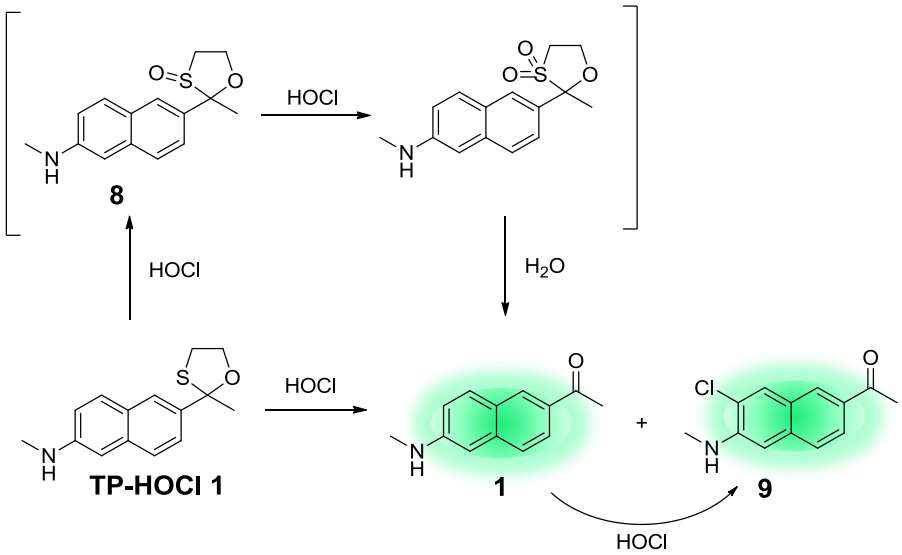

Figure 4. Proposed sensing mechanism of **TP-HOCl 1** for HOCl.

Fluorescence imaging of HOCl at sub-cellular level. HOCl, as the key "killer" for pathogens during phagocytosis, is proposed to be mainly produced from MPO-catalyzed peroxidation of chloride ions in phagolysosomes. Recently, accumulating research demonstrates that nonphagasomal HOCl (nphHOCl) can also be produced after incubation with soluble stimuli.[52,65] However, the organelles with intracellular nphHOCl are still unclear, which limits further elucidation of the corresponding functions of nphHOCl at sub-cellular level. Therefore, to clarify the distribution of HOCl at sub-cellular levels, mitochondria- (**MITO-TP**) and lysosome- (**LYSO-TP**) targetable derivatives of probe **TP-HOCl 1** were synthesized through introducing triphenylphosphine[61] or morpholine[60] to the amine group. Furthermore, *in vitro* experiment demonstrates that both **MITO-TP** and **LYSO-TP** can respond to HOCl at nanomolar level in PBS (1% DMSO, pH 7.4 and 5.0), respectively (Figure S12).

As shown in Figure S13, cell cytotoxicity of the probes was initially examined in HeLa cells, which proves that there is no significant cytotoxicity in the presence of 1–32 μM probe **MITO-TP** or **LYSO-TP** for 12 h. To determine the intracellular location of **MITO-TP** and **LYSO-TP** inside cells, the probe **MITO-TP** (or **LYSO-TP**) and Mito-Tracker Red (or Lyso-Tracker Red) were co-incubated with live

HeLa cells, which was treated HOCl (50 μM) for another 5 min. As expected, probe **MITO-TP** mainly localized in the mitochondria rather than lysosome and nucleus (Figure 5A and S14A), while **LYSO-TP** mainly stained in the lysosome of live cells (Figure 5B and S14B). Meanwhile, the same sub-cellular distribution of **MITO-TP** and **LYSO-TP** can also be confirmed in LPS/IFN-γ-stimulated macrophage

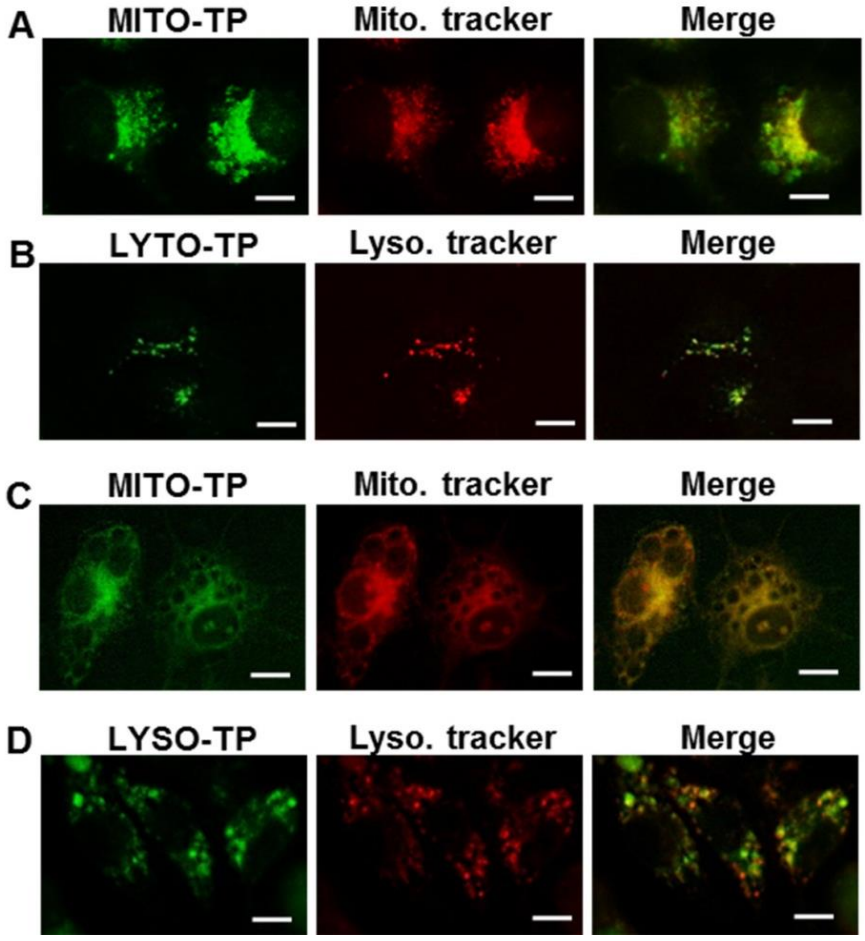

Figure 5. Intracellular localization of **MITO-TP** and **LYSO-TP** in HeLa (A, B) and macrophages cells (C, D). A, B) images of HeLa cells pre-treated with 10 μM **MITO-TP** (or 10 μM **LYSO-TP**) for 20 min and subsequently 1 μM Mito-Tracker Red (or 1 μM Lyso-Tracker Red) for 10 min. Then 50 μM HOCl was treated for another 5 min. C, D) images of macrophage cells pre-treated with LPS (120 ng / mL) / IFN-γ (20 ng / mL) for 24 h, then treated with 10 μM **MITO-TP** (or 10 μM **LYSO-TP**) for 20 min and subsequently 1 μM Mito-Tracker Red (or 1 μM Lyso-Tracker Red) for another 10 min. Green: probe fluorescence; red: Mito-Tracker and Lyso-Tracker fluorescence; yellow: merged signal. Scale bar: 10 μm.

cells (Figure 5C, D and S15). After confirming the intracellular localization of **LYSO-TP** and **MITO-TP**, the distribution time of these probes were evaluated in RAW cells (shown in Figure S16). To efficiently track the probes in cells, compound **4** and **7**, the bright fluorescent precursors of **LYSO-TP** and **MITO-TP** were used to examine the intracellular distribution time. As shown in Figure S16, the fluorescent intensity of compound **4** and **7** rapidly reaches the equilibrium state within 20 minutes in RAW cells and keeps stable in at least 60 min. Based on the structural similarity of probes (**LYSO-TP** and **MITO-TP**) and their precursors (**4** and **7**), it is rational to assume that the probes **LYSO-TP** and **MITO-TP** can also quickly reach the equilibrium state inside cells and keep stable for some time.

After that, the detection of HOCl in mitochondria and lysosome was examined in murine live macrophage cell line RAW 264.7 (Figure 6). It was reported that targeting groups such as triphenylphosphine[66] and morpholine[67,68] can significantly increase the distribution in mitochondria and lysosome respectively and relatively difficult to be washed out. Thus, RAW cells were incubated with **MITO-TP** and **LYSO-TP** for 20 min respectively and subsequently washed with PBS buffer to remove the free probes, which ensures that probes mainly localized in the targeted organelles (mitochondria and lysosome). As shown in Figure 6A (a, e), both **MITO-TP** and **LYSO-TP** stained cells showed very weak fluorescence. However, the intracellular fluorescence from both **MITO-TP** and **LYSO-TP** stained cells were much stronger when the cell was subsequently stimulated with Lipopolysaccharides (LPS, 1 μg/mL) and Phorbol Myristate Acetate (PMA, 1 μg/mL) together (Figure 6A (b, f) and Figure 6B-C). Based on remarkable fluorescence increase from the probe localized organelles, it is evident that the increased fluorescence signal is mainly due to the reaction between probes and non-phagosomal HOCl in mitochondria and lysosome.[65] To further examine the above assumption, control experiments were performed, in which 4-aminobenzoic acid hydrazide (ABH) was added to decrease cellular HOCl level through inhibiting the activity of MPO.[16] As shown in Figure 6A (c, g), cellular fluorescence intensity of both **MITO-TP**

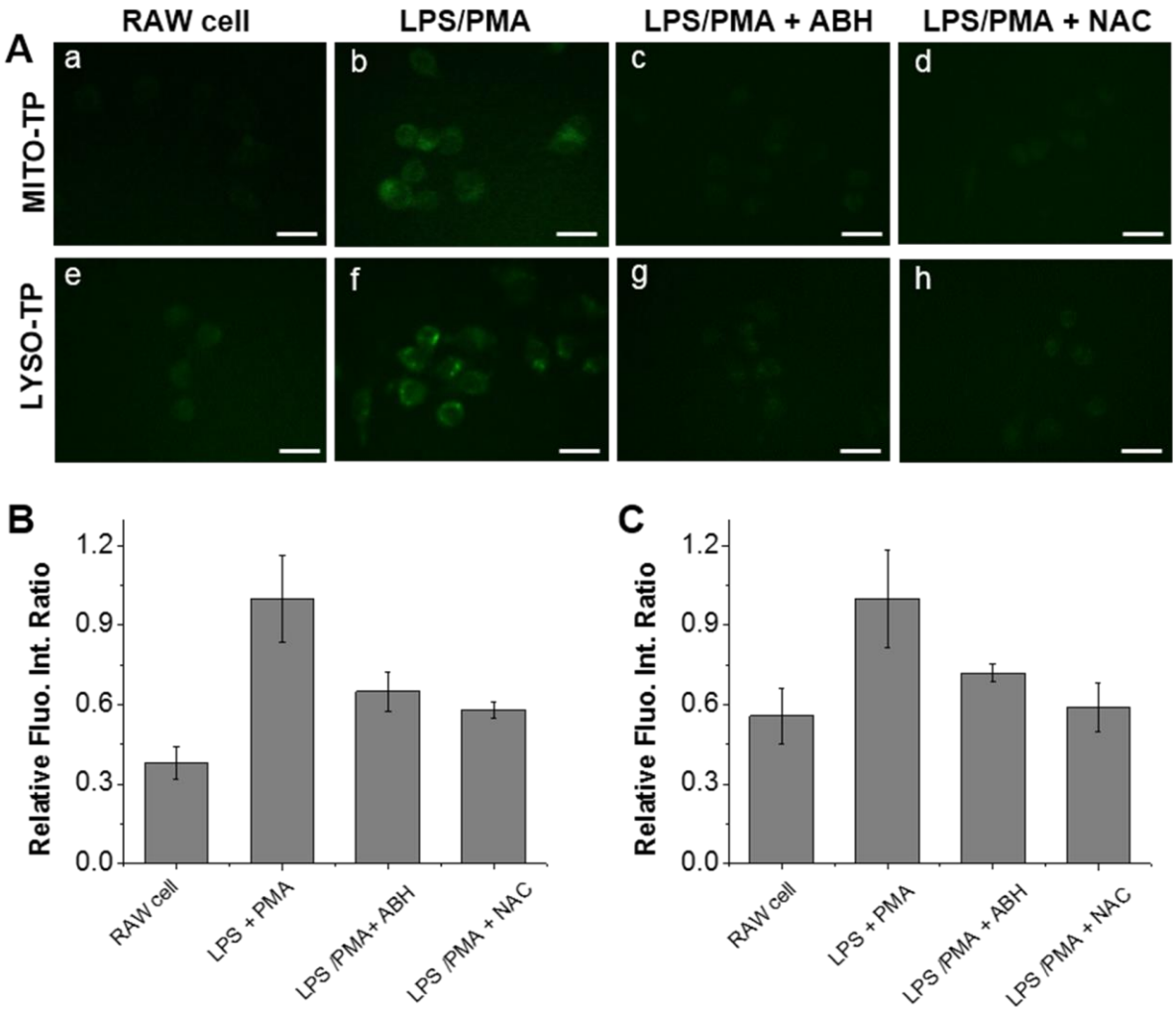

Figure 6. Detection of HOCl in live RAW 264.7 macrophage cells via **MITO-TP** and **LYSO-TP**. A) Representative fluorescent images of macrophage cells. a, e) **MITO-TP** or **LYSO-TP** (15 μM) was incubated with macrophages cells for 20 min and washed by PBS buffer. b, f) Cells were pre-incubated with probes, washed by PBS buffer and stimulated with LPS (1 μg/mL) / PMA (1 μg/mL) for 1 h. c, g) Cells were pre-incubated with probes, washed by PBS buffer and stimulated with LPS (1 μg/mL) / PMA (1 μg/mL) and ABH (200 μM) for 1 h . d, h) Cells were pre-incubated with probes, washed by PBS buffer and stimulated with LPS (1 μg/mL) / PMA (1 μg/mL) and NAC (1 mM) for 1 h. B, C) Quantification of the fluorescence signals from a-h. Data were normalized to the fluorescence intensity from LPS/PMA stimulated macrophage cells (b or f). Error bars are ± SD. n = 3. Scale bar: 30 μm.

and **LYSO-TP** stained cells is suppressed to some extent when the stimulated RAW cells were incubated with 200 μM ABH together. Similar phenomena were also observed in 24 h incubation of stimuli and ABH (Figure S17). In addition, the fluorescence of probes stained cells can also be reduced clearly by addition of N-acetylcysteine (NAC), a powerful ROS scavenger[71] (Figure 6A (d, h) and Figure 6B-C). This is mainly because most of the intracellular HOCl can be effectively removed by NAC, in which thiol atom can react with HOCl rapidly. One possible reason for the existence of intracellular HOCl in both mitochondrial and lysosomal is the movement of intracellular HOCl between organelles. Another plausible reason is that nphHOCl could be *in situ* generated in both mitochondria and lysosome of LPS/PMA-stimulated macrophage cells. This is because the respiratory burst induced by LPS and PMA in mitochondria produces higher amount of H_2O_2,[5,69,74] which can easily transfer to other organelles like the lysosome due to its good plasma membrane permeability.[70] Meanwhile, it is reported that MPO is located not only in lysosome but also in mitochondria of macrophage cells.[50,51] Therefore, it is assumed that H_2O_2 may work with MPO to produce nphHOCl in both mitochondria and lysosome.

Two-photon tissue imaging of HOCl in inflamed mouse model. To examine whether nphHOCl can be *in vivo* detected in mitochondria and lysosome of macrophage cells in inflamed mouse model, 200 μL LPS (1 mg/mL) was subcutaneously injected into right rear paws of mouse to cause inflammation (Figure 7A). After 1 day, **MITO-TP** and **LYSO-TP** were intravenously injected and the paw skin was sectioned 1 hour later. As shown in Figure 7B, strong fluorescence from both **MITO-TP** and **LYSO-TP** in LPS-stimulated macrophage cells was observed in inflammation tissues (shown in green color), which was further confirmed by immune-staining histological sections with macrophage marker CD11b (shown in red color). However, the signals from both probes and macrophage marker remained largely negative in the normal tissues (Figure 7B and Figure S18).

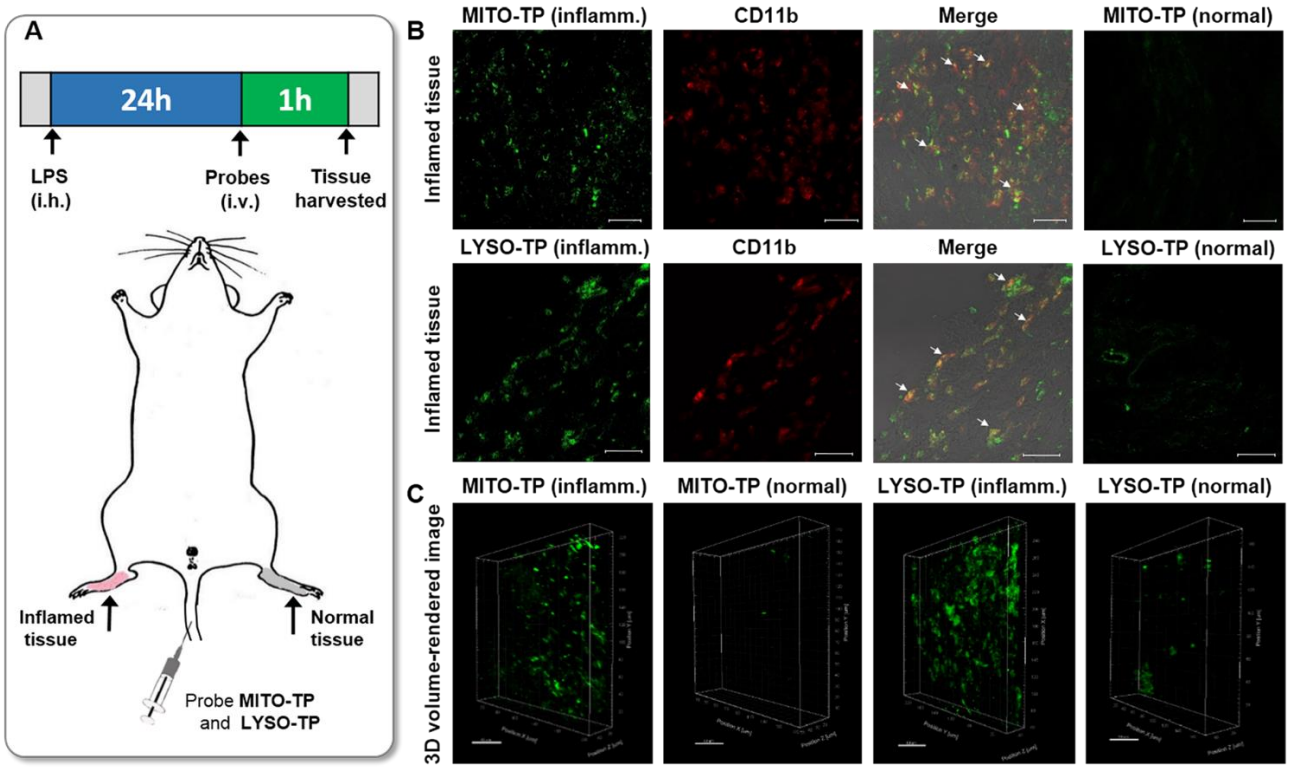

Figure 7. Detection of LPS-dependent HOCl generation in inflammation tissues via **LYSO-TP** and **MITO-TP**. A) 200 μL LPS (1 mg/mL) was subcutaneously (i.h.) injected into right rear paws of mouse to cause inflammation. After 1 day, 200 μL of 1 mM **MITO-TP** (or **LYSO-TP**) was intravenously (i.v.) injected and the paw skin was sectioned 1 hour later. B) Fluorescence images of probes and CD11b in the inflamed tissue. Probe fluorescence: green, antibody CD11b: red. Arrows indicates the merged parts of HOCl sensitive probes and CD11b. C) 3D volume-rendered image shows the distribution of macrophages within the inflamed and normal tissues. (+): inflammation tissues; (-): normal tissues; Scale bar: 30 μm.

Besides, the fluorescence from **MITO-TP** and **LYSO-TP** was collected at different depth in inflamed tissues and reconstructed in 3D box to describe the spatial distribution of LPS-stimulated macrophage cells (Figure 7C). Taken together, **MITO-TP** and **LYSO-TP** was successfully applied to stain the macrophage cells in inflamed mouse model through intravenous injection. Importantly, it is indicated that

much higher concentration of nphHOCl in both mitochondria and lysosome of macrophage cells could be detected during inflammation.

Conclusion

In summary, we have developed the first two-photon fluorescent "turn-on" HOCl probe (**TP-HOCl 1**) and its mitochondria (**MITO-TP**) and lysosome (**LYSO-TP**) targetable derivatives to image HOCl among corresponding organelles. Because of the unique oxidation de-protection mechanism, these probes show not only fast response (within seconds) and good sensitivity (< 20 nM) to HOCl but also high selectivity over other ROS and bio-molecules. Cell imaging experiments indicate that probes **MITO-TP** and **LYSO-TP** display good cell penetration and localize in mitochondria and lysosome of living cells respectively. Furthermore, it was indicated that HOCl may be detected in both mitochondria and lysosome of LPS/PMA-stimulated macrophage cells. In particular, two-photon imaging shows that much larger amount of HOCl can be detected in both lysosome and mitochondria of macrophage cells during inflammation condition in murine model. Therefore, due to the advantages of these probes, they can not only help elucidate the distribution of sub-cellular HOCl, but also serve as excellent tools to exploit potential functions of HOCl at sub-cellular and tissue levels.

ASSOCIATED CONTENT

Synthesis, additional spectroscopic and imaging data, Gaussian calculation results, and MTT results. This material is available free of charge via the Internet at http://pubs.acs.org.

AUTHOR INFORMATION

Corresponding Author

* chmcyt@nus.edu.sg

Author Contributions

‡These authors contributed equally.

Notes

The authors declare no competing financial interest.

ACKNOWLEDGMENT

This work was supported by intramural funding from A*STAR (Agency for Science, Technology and Research, Singapore) Biomedical Research Council and National Medical Research Council grant (NMRC/CBRG/0015/2012).

ABBREVIATIONS

ROS, reaction oxygen species; HOCl, hypochlorous acid; MPO, myeloperoxidase; nphHOCl, nonphagosomal intracellular HOCl; TPM, two-photon microscope; ABH, 4-aminobenzoic acid; LPS, lipopolysaccharide; IFN –γ, interferon γ; NAC, N-acetylcysteine.

REFERENCES

(1) Finkel, T.; Holbrook, N. J. *Nature* **2000**, *408*, 239.
(2) Branzk, N.; Lubojemska, A.; Hardison, S. E.; Wang, Q.; Gutierrez, M. G.; Brown, G. D.; Papayannopoulos, V. *Nat. Immunol.* **2014**, *15*, 1017.
(3) Strowig, T.; Henao-Mejia, J.; Elinav, E.; Flavell, R. *Nature* **2012**, *481*, 278.
(4) Winterbourn, C. C.; Hampton, M. B.; Livesey, J. H.; Kettle, A. J. *J. Biol. Chem.* **2006**, *281*, 39860.
(5) Klebanoff, S. J. *J. Leukoc. Biol.* **2005**, *77*, 598.
(6) Koide, Y.; Urano, Y.; Hanaoka, K.; Terai, T.; Nagano, T. *J. Am. Chem. Soc.* **2011**, *133*, 5680.
(7) Kobayashi, T.; Robinson, J. M.; Seguchi, H. *J. Cell Sci.* **1998**, *111 (Pt 1)*, 81.
(8) Whiteman, M.; Rose, P.; Siau, J. L.; Cheung, N. S.; Tan, G. S.; Halliwell, B.; Armstrong, J. S. *Free Radic. Biol. Med.* **2005**, *38*, 1571.
(9) Matute, J. D.; Arias, A. A.; Wright, N. A.; Wrobel, I.; Waterhouse, C. C.; Li, X. J.; Marchal, C. C.; Stull, N. D.; Lewis, D. B.; Steele, M.; Kellner, J. D.; Yu, W.; Meroueh, S. O.; Nauseef, W. M.; Dinauer, M. C. *Blood* **2009**, *114*, 3309.
(10) Yap, Y. W.; Whiteman, M.; Cheung, N. S. *Cell Signal* **2007**, *19*, 219.
(11) Choi, D. K.; Pennathur, S.; Perier, C.; Tieu, K.; Teismann, P.; Wu, D. C.; Jackson-Lewis, V.; Vila, M.; Vonsattel, J. P.; Heinecke, J. W.; Przedborski, S. *J. Neurosci.* **2005**, *25*, 6594.
(12) Miljkovic-Lolic, M.; Silbergleit, R.; Fiskum, G.; Rosenthal, R. E. *Brain Res.* **2003**, *971*, 90.
(13) Yang, Y. T.; Whiteman, M.; Gieseg, S. P. *Biochim. Biophys. Acta.* **2012**, *1823*, 420.

(14) Yap, Y. W.; Whiteman, M.; Bay, B. H.; Li, Y.; Sheu, F. S.; Qi, R. Z.; Tan, C. H.; Cheung, N. S. *J. Neurochem.* **2006**, *98*, 1597.

(15) Bylund, J.; Brown, K. L.; Movitz, C.; Dahlgren, C.; Karlsson, A. *Free Radic. Biol. Med.* **2010**, *49*, 1834.

(16) Klebanoff, S. J.; Kettle, A. J.; Rosen, H.; Winterbourn, C. C.; Nauseef, W. M. *J. Leukoc. Biol.* **2013**, *93*, 185.

(17) Winterbourn, C. C. *Toxicology* **2002**, *181*, 223.

(18) Aratani, Y.; Koyama, H.; Nyui, S.; Suzuki, K.; Kura, F.; Maeda, N. *Infect. Immun.* **1999**, *67*, 1828.

(19) J Cell SciFernandez-Suarez, M.; Ting, A. Y. *Nat. Rev. Mol. Cell. Biol.* **2008**, *9*, 929.

(20) Chan, J.; Dodani, S. C.; Chang, C. J. *Nat. Chem.* **2012**, *4*, 973.

(21) Dickinson, B. C.; Chang, C. J. *J. Am. Chem. Soc.* **2008**, *130*, 9638.

(22) Lim, S. Y.; Hong, K. H.; Kim, D. I.; Kwon, H.; Kim, H. J. *J. Am. Chem. Soc.* **2014**, *136*, 7018.

(23) Lee, M. H.; Park, N.; Yi, C.; Han, J. H.; Hong, J. H.; Kim, K. P.; Kang, D. H.; Sessler, J. L.; Kang, C.; Kim, J. S. *J. Am. Chem. Soc.* **2014**, *136*, 14136.

(24) Ishida, M.; Watanabe, H.; Takigawa, K.; Kurishita, Y.; Oki, C.; Nakamura, A.; Hamachi, I.; Tsukiji, S. *J. Am. Chem. Soc.* **2013**, *135*, 12684.

(25) Arai, S.; Lee, S.-C.; Zhai, D.; Suzuki, M.; Chang, Y. T. *Sci. Rep.* **2014**, *4*, 6701.

(26) Kim, H. M.; Cho, B. R. *Acc. Chem. Res.* **2009**, *42*, 863.

(27) Helmchen, F.; Denk, W. *Nat. Methods* **2005**, *2*, 932.

(28) Kim, D.; Ryu, H. G.; Ahn, K. H. *Org. Biomol. Chem.* **2014**, *12*, 4550.

(29) Yuan, L.; Jin, F.; Zeng, Z.; Liu, C.; Luo, S; Wu, J. *Chem. Sci.* **2015**, DOI: 10.1039/C4SC03883E.

(30) Chen, X.; Wang, X.; Wang, S.; Shi, W.; Wang, K.; Ma, H. *Chem. Eur. J.* **2008**, *14*, 4719.

(31) Sun, Z. N.; Liu, F. Q.; Chen, Y.; Tam, P. K.; Yang, D. *Org. Lett.* **2008**, *10*, 2171.

(32) Hu, J. J.; Wong, N. K.; Gu, Q.; Bai, X.; Ye, S.; Yang, D. *Org. Lett.* **2014**, *16*, 3544.

(33) Lin, W.; Long, L.; Chen, B.; Tan, W. *Chem. Eur. J.* **2009**, *15*, 2305.

(34) Cheng, X.; Jia, H.; Long, T.; Feng, J.; Qin, J.; Li, Z. *Chem. Commun.* **2011**, *47*, 11978.

(35) Emrullahoglu, M.; Ucuncu, M.; Karakus, E. *Chem. Commun.* **2013**, *49*, 7836.

(36) Zhao, N.; Wu, Y. H.; Wang, R. M.; Shi, L. X.; Chen, Z. N. *Analyst* **2011**, *136*, 2277.

(37) Cheng, G.; Fan, J.; Sun, W.; Cao, J.; Hu, C.; Peng, X. *Chem. Commun.* **2014**, *50*, 1018.

(38) Liu, S. R.; Wu, S. P. *Org. Lett.* **2013**, *15*, 878.

(39) Li, G.; Zhu, D.; Liu, Q.; Xue, L.; Jiang, H. *Org. Lett.* **2013**, *15*, 2002.

(40) Qu, Z.; Ding, J.; Zhao, M.; Li, P. *J. Photoch. Photobio. A* **2015**, *299*, 1.

(41) Zhan, X.-Q.; Yan, J.-H.; Su, J.-H.; Wang, Y.-C.; He, J.; Wang, S.-Y.; Zheng, H.; Xu, J.-G. *Sensor. Actuat. B: Chem.* **2010**, *150*, 774.

(42) Chen, X.; Lee, K. A.; Ha, E. M.; Lee, K. M.; Seo, Y. Y.; Choi, H. K.; Kim, H. N.; Kim, M. J.; Cho, C. S.; Lee, S. Y.; Lee, W. J.; Yoon, J. *Chem. Commun.* **2011**, *47*, 4373.

(43) Xu, Q.; Lee, K. A.; Lee, S.; Lee, K. M.; Lee, W. J.; Yoon, J. *J. Am. Chem. Soc.* **2013**, *135*, 9944.

(44) Wu, X. J.; Li, Z.; Yang, L.; Han, J. H.; Han, S. F. *Chem. Sci.* **2013**, *4*, 460.

(45) Zhang, R.; Ye, Z.; Song, B.; Dai, Z.; An, X.; Yuan, J. *Inorg. Chem.* **2013**, *52*, 10325.

(46) Xiao, H.; Xin, K.; Dou, H.; Yin, G.; Quan, Y.; Wang, R. *Chem. Commun.* **2015**, *51*, 1442.

(47) Ye, Z.; Zhang, R.; Song, B.; Dai, Z.; Jin, D.; Goldys, E. M.; Yuan, J. *Dalton Trans.* **2014**, *43*, 8414.

(48) Yuan, L.; Lin, W.; Xie, Y.; Chen, B.; Song, J. *Chem. Eur. J.* **2012**, *18*, 2700.

(49) Zhu, H.; Fan, J.; Wang, J.; Mu, H.; Peng, X. *J. Am. Chem. Soc.* **2014**, *136*, 12820.

(50) Nauseef, W. M. *Blood* **1987**, *70*, 1143.

(51) de Araujo, T. H.; Okada, S. S.; Ghosn, E. E.; Taniwaki, N. N.; Rodrigues, M. R.; de Almeida, S. R.; Mortara, R. A.; Russo, M.; Campa, A.; Albuquerque, R. C. *Cell Immunol.* **2013**, *281*, 27.

(52) Li, G.; Lin, Q.; Ji, L.; Chao, H. *J. Mater. Chem. B* **2014**, *2*, 7918.

(53) Wu, X.; Li, Z.; Yang, L.; Han, J.; Han, S. *Chem. Sci.* **2013**, *4*, 460.

(54) Kim, H. M.; Seo, M. S.; An, M. J.; Hong, J. H.; Tian, Y. S.; Choi, J. H.; Kwon, O.; Lee, K. J.; Cho, B. R. *Angew. Chem. Int. Ed.* **2008**, *47*, 5167.

(55) Rao, A. S.; Kim, D.; Nam, H.; Jo, H.; Kim, K. H.; Ban, C.; Ahn, K. H. *Chem. Commun.* **2012**, *48*, 3206.

(56) Rao, A. S.; Kim, D.; Wang, T.; Kim, K. H.; Hwang, S.; Ahn, K. H. *Org. Lett.* **2012**, *14*, 2598.

(57) Kim, H. M.; An, M. J.; Hong, J. H.; Jeong, B. H.; Kwon, O.; Hyon, J. Y.; Hong, S. C.; Lee, K. J.; Cho, B. R. *Angew. Chem. Int. Ed.* **2008**, *47*, 2231.

(58) Hawkins, C. L.; Pattison, D. I.; Davies, M. J. *Amino Acids* **2003**, *25*, 259.

(59) Reja, S. I.; Bhalla, V.; Sharma, A.; Kaur, G.; Kumar, M. *Chem. Commun.* **2014**, *50*, 11911.

(60) Yu, H.; Xiao, Y.; Jin, L. *J. Am. Chem. Soc.* **2012**, *134*, 17486.

(61) Lee, M. H.; Han, J. H.; Lee, J. H.; Choi, H. G.; Kang, C.; Kim, J. S. *J. Am. Chem. Soc.* **2012**, *134*, 17314.

(62) Oakes, J.; Gratton, P. *J. Chem. Soc.-Perk. T. 2* **1998**, 2201.

(63) Xiao, H.; Xin, K.; Dou, H.; Yin, G.; Quan, Y.; Wang, R. *Chem. Commun.* **2015**, *51*, 1442.

(64) Zhang, Y. R.; Chen, X. P.; Jing, S.; Zhang, J. Y.; Yuan, Q.; Miao, J. Y.; Zhao, B. X. *Chem. Commun.* **2014**, *50*, 14241.

(65) Muijsers, R. B.; van Den Worm, E.; Folkerts, G.; Beukelman, C. J.; Koster, A. S.; Postma, D. S.; Nijkamp, F. P. *Br. J. Pharmacol.* **2000**, *130*, 932.

(66) Murphy, M. P.; Smith, R. A. *Annu. Rev. Pharmacol. Toxicol.* **2007**, *47*, 629.

(67) de Duve, C.; de Barsy, T.; Poole, B.; Trouet, A.; Tulkens, P.; Van Hoof, F. *Biochem. Pharmacol.* **1974**, *23*, 2495.

(68) Firestone, R. A.; Pisano, J. M.; Bonney, R. J. *J. Med. Chem.* **1979**, *22*, 1130.

(69) Schroder, K.; Hertzog, P. J.; Ravasi, T.; Hume, D. A. *J. Leukoc. Biol.* **2004**, *75*, 163.

(70) Henzler, T.; Steudle, E. *J. Exp. Bot.* **2000**, *51*, 2053.

(71) Witko-Sarsat, V.; Gausson, V.; Nguyen, A. T.; Touam, M.; Drueke, T.; Santangelo, F.; Descamps-Latscha, B. *Kidney Int.* **2003**, *64*, 82.

(72) Kenmoku, S.; Urano, Y.; Kojima, H.; Nagano, T . *J. Am. Chem. Soc.* **2007,** *129*, 7313.

(73) Hou, J.-T.; Wu, M.-Y.; Li, K.; Yang, J.; Yu, K.-K.; Xie, Y.-M.; Yu, X.-Q. *Chem. Commun.* **2014,** *50*, 8640.

(74) Michaelis, J.; Vissers, M. C.; Winterbourn, C. C. *Arch. Biochem. Biophys.* **1992,** *2*, 555.

TOC

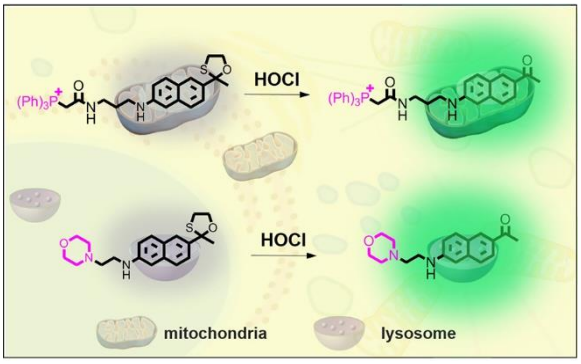

Development of Targetable Two-Photon Fluorescent Probes to Image Hypochlorous Acid in Mitochondria and Lysosome in Live Cell and Inflamed Mouse Model

Lin Yuan[1,2‡], Lu Wang[1‡], Bikram Keshari Agrawalla[1], Sung-Jin Park[3], Hai Zhu[1], Balasubramaniam Sivaraman[3], Juanjuan Peng[3], Qing-Hua Xu[1], Young-Tae Chang[1,3]*

[1]Department of Chemistry, National University of Singapore, Singapore 117543

[2]State Key Laboratory of Chemo/Biosensing and Chemometrics, College of Chemistry and Chemical Engineering, Hunan University, Changsha 410082, PR China

[3]Laboratory Bioimaging Probe Development, Singapore Bioimaging Consortium, Singapore 117543.

Supporting Information

Table of content

1. Supplemental Figures and Tables S3-17
2. Materials and General Experimental Methods. S17
3. Synthesis and Characterization S18–20
4. Photospectroscopic Studies S21
5. Analytical HPLC analysis S21
6. *In Vitro* Fluorescence Microscopic Studies S22
7. Two-photon Tissue Imaging Studies S23
8. Supplemental Spectra S24-33
9. Reference S33-34

1. Supplemental Figures and Tables

Table S1. Properties of respresentive fluorescent HOCl probes

Probes[i]	$\lambda_{ab}/\lambda_{em}$ nm[a] and FEF[b]	Sensing moieties[c]	Detection limit/nM[d]	Reaction time[e]	Solution[f] and worked pH range[g]	Imaging application[h]
N-benzoyl rhodamine B–hydrazide[1]	554/578; --	dibenzoylhydrazine	27	30 min	$Na_2B_4O_7$/NaOH buffer (pH 12); pH range: pH > 9.0	--
HySOx[2]	555/575; --	thioether	--	within seconds	PBS (pH 7.4, 0.10 to 20% DMF); pH range: 4.0–9.0	Endogenous / porcine neutrophil
MMSiR[3]	652/670; --	thioether	--	within seconds	PBS (pH 7.4); pH range: 4.0-9.0	Endogenous / model mouse
Rhodamine B thiospirolactone[4]	555/579; --	internal thioester	300	within 5 min	PBS (pH 7.4, 10% DMSO); pH range: 3.0-8.0	Endogenous / neutrophils and fresh kidney sections
R19-S[5]	--/550; --	internal thioester	--	--	KH_2PO_4 buffer/CH_3CN (pH 5.5, 99:1); --	Endogenous / neutrophils and intestinal epithelia
FBS[6]	~498/523;	internal thioester and boronate	200	within 1 min	KH_2PO_4 buffer (pH 7.4); pH range: ≥ 5.5	Endogenous / intestinal epithelia of *Drosophila*.
$[Ru(bpy)_2(DNPS\text{-}bpy)]\text{-}(PF_6)_2$[7]	450/626; ~190-fold	thioether	53.5	--	PBS (pH 7.4); pH range: 4.5–10.5	Endogenous / RAW 264.7 cells
$Ru(bpy)_2(AN\text{-}bpy)](PF_6)_2$[8]	456/612; ~110-fold	ether	33	within 10 min	borate buffer (pH 7.4); pH range: 3.0–10.0	Endogenous / porcine neutrophils
Cou-Rho-HOCl[9]	410/473-594	thiosemicarbazide	52	within minuties	PBS/DMF (pH 7.4, 1:1); pH range: 3.0–11.0	Endogenous / RAW 264.7 cells
HKOCl-1[10]	--/541; ~1079-fold	p-methoxyphenol.	--	--	PBS (pH 7.5) ; pH range: 5.0-8.0	Endogenous / RAW 264.7 macrophages
HKOCl-2a[11]	--/525; ~765-fold	p-methoxyphenol.	42	within 15 min	PBS (pH 7.4) --	--
HKOCl-2b[11]	--/523; ~900-fold	p-methoxyphenol.	18	within 15 min	PBS (pH 7.4); pH range of 4-10	Endogenous / macrophages
HKOCl-2c[11]	--/525; ~274-fold	p-methoxyphenol.	37	within 15 min	PBS (pH 7.4) --	--
Phenanthroimidazole- oxime[12]	--/509-439; ~9.8-fold (ratio)	oxime	--	within seconds	PBS/DMF (pH 9.0, 1:4); pH range: > 8.5	--
Flu-1[13]	--/530; ~61-fold	oxime	--	within seconds	HEPES/DMSO (pH 7.05, 1:9); pH range: 7.0–10.0	Exogenous / HeLa cell
Bodipy-OX[14]	502/529; ~48-fold	oxime	500	within seconds	PBS/DMF (pH 7.2, 4:1) pH range: 4.0–9.0	Exogenous / MCF10A cell
$Ir(ppy)_2(L_1)](PF_6)$[15]	346/578; ~31-fold	oxime	≈ 13 (1 ppm)	--	DMF/HEPES (pH 7.2, 4 : 1) pH range: 2.0–13.0	--
BClO[16]	500/505; ~100-fold	pyrrole	0.56	within 1 s	PBS/EtOH (pH 7.4, 1:9); pH range: 4.0–9.0	Endogenous / MCF-7 cells
SeCy7[17]	--/786; ~19.4-fold	selenide	310	within dozens of seconds	PBS buffer (pH 7.4); pH range: 4.0-10.0	Endogenous / model mouse
HCSe[18]	--/526; --	selenide	7.98	within 4 minuties	MPBS /CH_3CN (pH7.4, 99/1); pH range: 5.5-8.0	Endogenous / RAW264.7 cells

CM1[19]	405/480; ~63-fold	selenide	10	within seconds	PBS (pH=7.4); pH range: 4.0-9.0	Endogenous / RAW264.7 cells
Lyso-NI-Se[20]	450/540 ~22-fold	selenide	18.5	within seconds	CH3CN/H2O (pH 5.0, 1:1); pH range: 2.5-8.5	Exogenous / lysosome of Raw 264.7 cell
ThioRB-FITC-MSN[21]	490/526,586 ~7-fold (ratio)	internal thioester	--	within seconds	Na2HPO4/citrate buffer (pH 5.0); pH range: 4.5-8.0	Exogenous / lysosome of Raw 264.7 cell
PZ–Py[22]	400/562 ~40.5-fold	thioether	17.9	within seconds	PBS (pH 7.3) pH range: 4.0-10.0	Endogenous / mitochondria of RAW 264.7 cells and nude mice
Ir2[23]	405/565 ~12.8-fold	diaminomaleonitrile-functionalized Schiff base	--	within seconds	DMF/PBS buffer (pH 7.4, 3:7); pH range: 4.0-10.0	Exogenous / mitochondria of Raw 264.7 cells and Hela cells
Rh-Py[24]	544/577 ~380-fold	dibenzoylhydrazine	24	within seconds	PBS (pH 7.4) pH range: 4.0-10.0	Exogenous / mitochondria of HeLa cells and nude mice
TP-HOCl 1[25]	375/500 ~670-fold	1,3-oxathiolane	16.6	within seconds	PBS/EtOH (1:1, PH 7.4) pH range: 4.0-9.0	--
MITO-TP[25]	375/500 ~634-fold	1,3-oxathiolane	17.2	within seconds	PBS (PH 7.4) --	Endogenous / mitochondria of Raw 264.7 cells and inflamed tissues
LYSO-TP[25]	375/500 ~610-fold	1,3-oxathiolane	19.6	within seconds	PBS (PH 5.0) --	Endogenous / lysosome of Raw 264.7 cells and inflamed tissues

[a] Absorption and emission wavelength. [b] The fluorescence enhanced factor or emission ratio changes before and after interaction with HOCl. [c] The recognition moieties that respond to HOCl. [d] The reported detection limit of corresponding probes. [e] The reaction time for responding to HOCl. [f] The solution and pH used for spectrum measurement. [g] The worked pH range for responding to HOCl. [h] Imaging of endogenous or exogenous HOCl. [i] In recent years, some fluorescent probes with high selectivity and sensitivity, fast response, and wide range of working pH have been developed for the detection of HOCl in biological system. The design strategies for developing HOCl probes are based on specific reactions between HOCl and recognition sites, which changes fluorescence intensity significantly before and after reaction. Based on the reference, the recognition moieties include p-methoxyphenol[10,11], dibenzoylhydrazine,[1] oxime,[12-15] selenide,[17-20] thiol (tetrahydrothiophene/thioether[2-3,7,22], internal thioester[4-6,21] and thiosemicarbazide[9]) and other groups.[8,16] Most of the probes can respond to HOCl with good sensitivity (usually dozens of nM) in a very short reaction time (usually from seconds to minutes). Some probes were successfully applied in real-time detection of endogenous HOCl insides cells and a small number of probes were used to image HOCl in inflamed tissues of mice. Among these probes, several organelles (mitochondria[22-24] and lysosome[20-21]) targetable probes have been reported since 2013. The endogenous mitochondrial HOCl was successfully detected by PZ–Py,[22] which was developed by Wang's group. However, the detection of endogenous HOCl in lysosome has not been reported in existing papers, even two lysosomal probes were developed. In addition, no report exists describing a TPM (two-photon microscopy) based probe for direct imaging of endogenous HOCl produced in both live cells and tissues. Therefore, considering greater tissue penetration depths, higher spatial resolution, and lower photo-toxicity of TPM, organelles targetable two-photon probes can be a useful tool to elucidate the functions of HOCl in biological system.

Table S2. Photophysical parameters of fluorophores.

Dye	$\lambda_{max\ OP}$ (nm)[a]	$\varepsilon_{max\ SP}$ ($10^4 cm^{-1}mol^{-1}$)[b]	Φ[c]	$\lambda_{max\ TP}$ (nm)[d]	$\Phi\sigma_{max}$ [GM][e]
1	356	1.26	0.40	750	82
TP-HOCl 1	356	1.23	<0.001	750	n.d.[f]
7	356	1.24	0.41	750	83
MITO-TP	356	1.22	<0.001	750	n.d.[f]
4	356	1.25	0.35	750	74
LYTO-TP	356	1.23	<0.001	750	n.d.[f]
8	356	1.24	<0.001	750	n.d.[f]
9	356	1.27	0.38	750	79

[a] Maximum one photon absorbance wavelength of fluorophores in MeOH. [b] The molar extinction coefficients at λ_{max}. [c] Fluorescence quantum yield. [d] Maximum two photon-excitation wavelength. [e] The peak of two-photon-action cross-section (GM: 10^{-50} cm^4 s $photon^{-1}$). [f] n.d.: not determined. The two-photon emission intensity was too weak to measure the cross-section accurately.

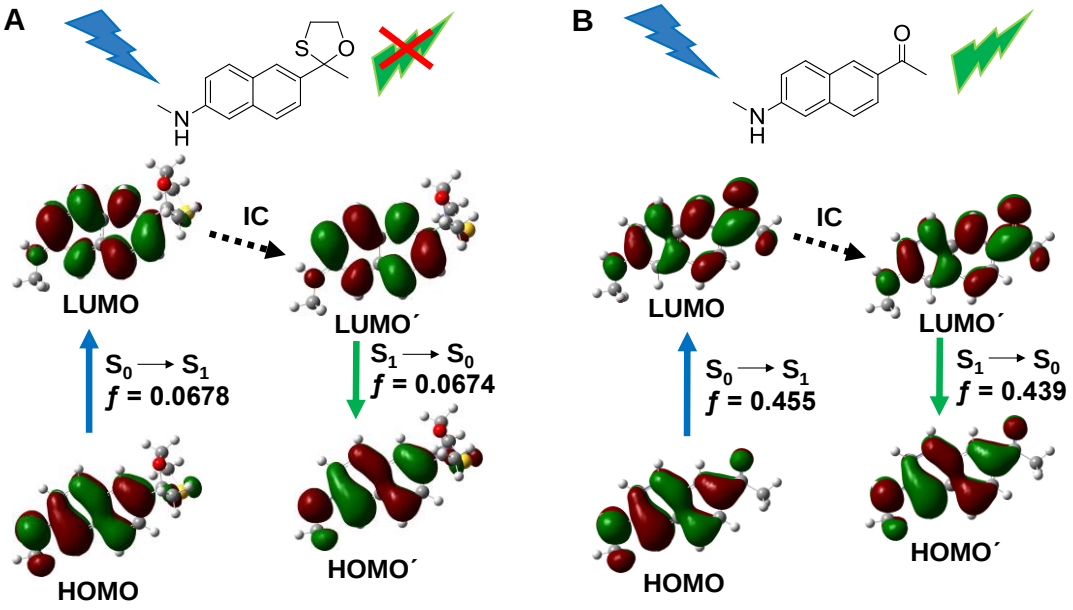

Figure S1. The frontier molecular orbitals (MOs) of **TP-HOCl 1** (A) and compound **1** (B) involved in the vertical excitation (i.e. UV-vis absorption, the left columns) and emission (right columns) shown in solid line. Methanol (CPCM model) was employed as the solvent for the DFT calculations. The vertical excitation related calculations are based on the optimized ground state (S_0 state), the emission related calculations were based on the optimized excited state (S_1 state), at the B3LYP/6-31G (d)/level using Gaussian 09W. IC stands for internal conversion (dotted lines).

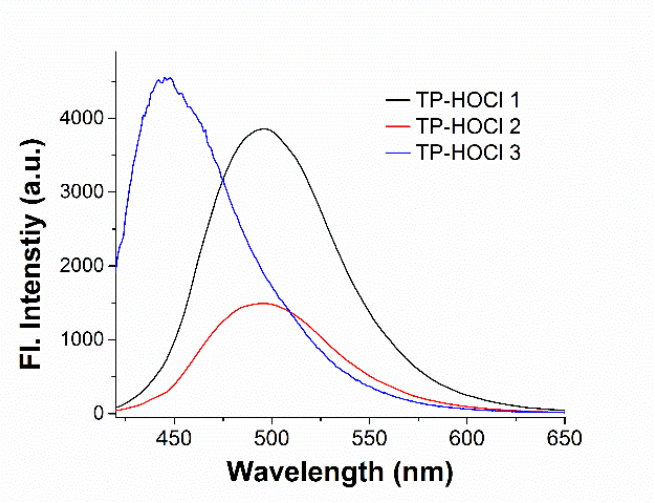

Figure S2. The emission spectra of three probes (5μM) after adding 50 μM HOCl. Excitation wavelength: 375 nm.

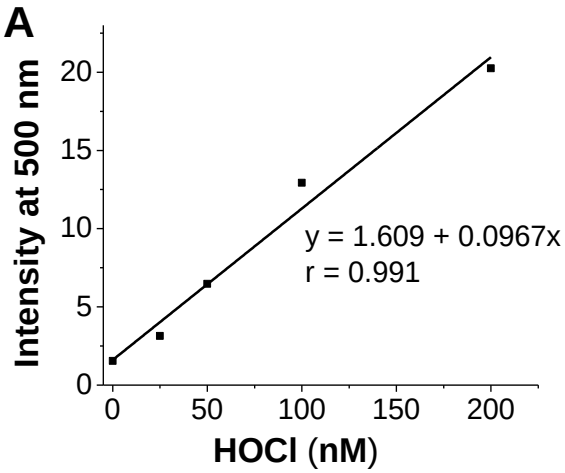

Figure S3. The linear fluorescence response of **TP-HOCl 1** to the concentration of HOCl at the nanomolar concentration range (0-200 nM).

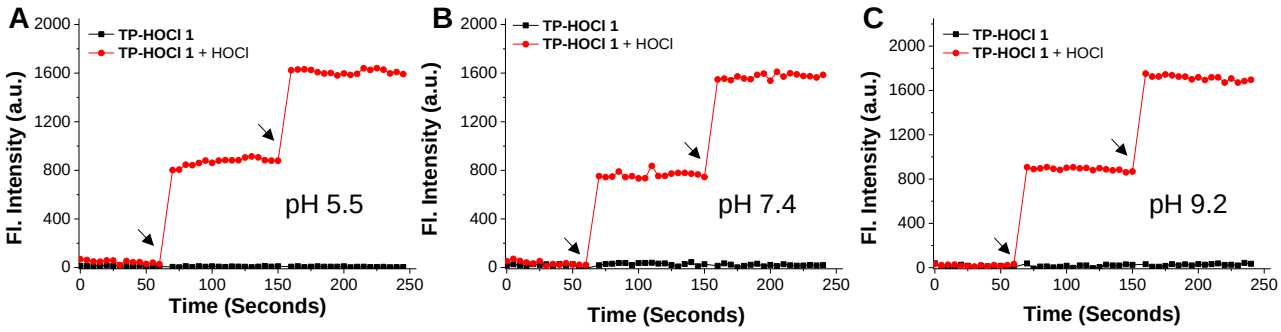

Figure S4. **TP-HOCl 1** can respond to HOCl within seconds at pH 5.5 (A), 7.4 (B) and 9.2 (B). Arrows indicate the addition of 25 μM HOCl.

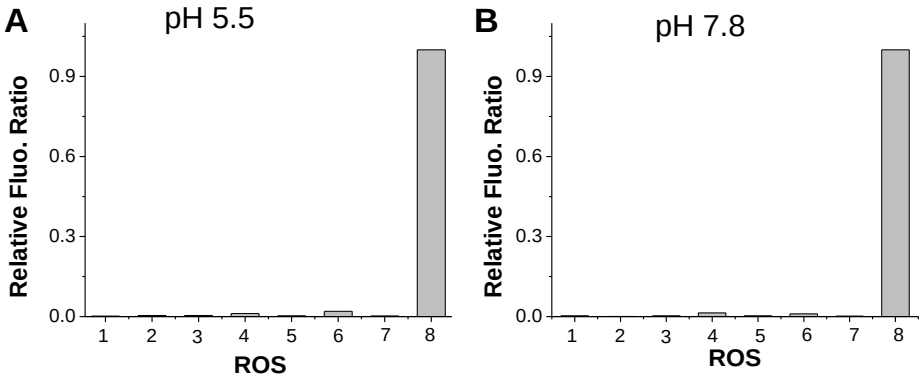

Figure S5. Fluorescence response of **TP-HOCl 1** (5 μM) towards various ROS (50 μM for HOCl (8) and 250 μM for other ROS/RNS (1-7)) at pH 5.5 (A) and 7.8 (B). 1) H_2O_2; 2) •OH; 3) O^{2-}; 4) NO•; 5) *t*-BuOOH; 6) *t*-BuOO•; 7) $ONOO^-$; 8) HOCl.

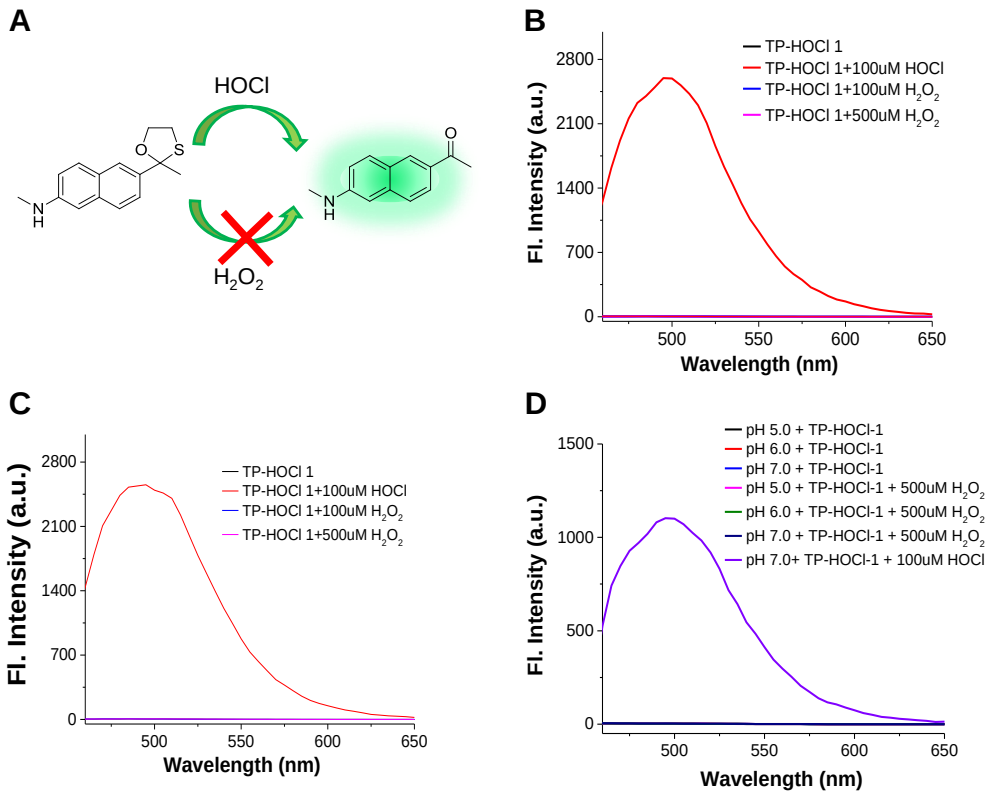

Figure S6. The fluorescence spectra of **TP-HOCl 1** (5 μM) after adding HOCl (100 μM) and H_2O_2 (100 and 500 μM) in EtOH (B) and PBS/MeOH (1 : 1) solution (C). D) **TP-HOCl 1** kept stable in the presence of H_2O_2 (500 μM) in PBS (pH 5.0, 6.0, 7.0).

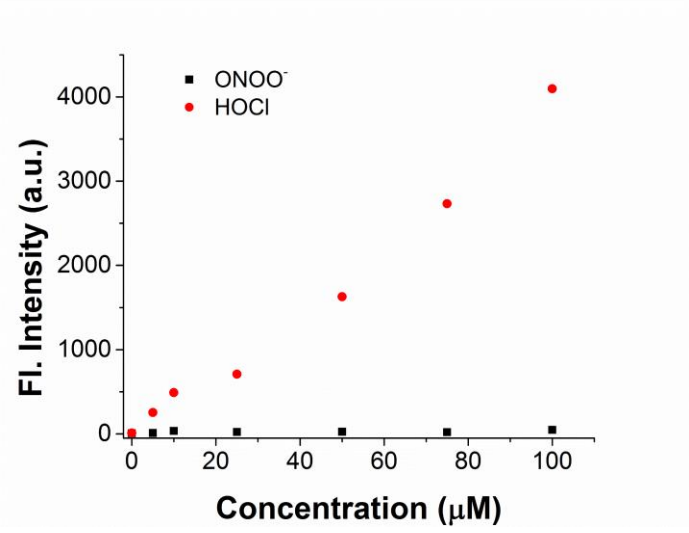

Figure S7. Fluorescence intensity of **TP-HOCl 1** (5 μM) before and after adding HOCl (●) or $ONOO^-$ (■) at different concentrations (0 to 100 μM).

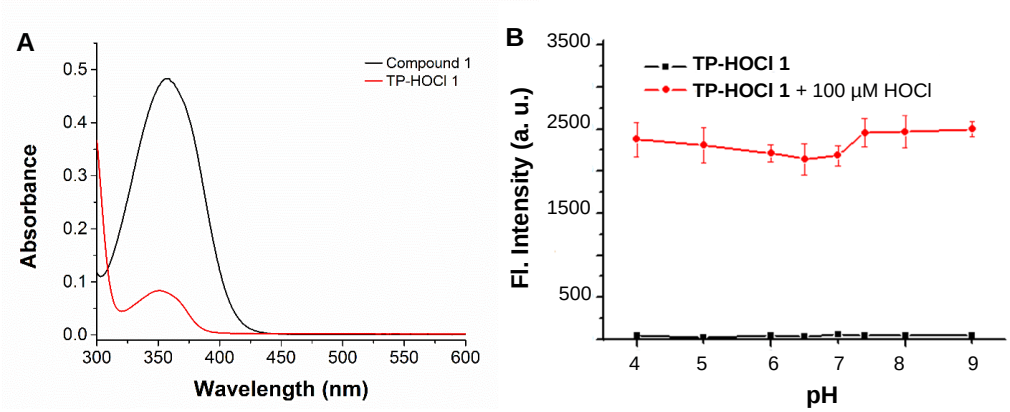

Figure S8. A) The absorption spectra of **TP-HOCl 1** and de-protected compound **1** in MeOH. B) The fluorescence spectra of **TP-HOCl 1** before and after addition of HOCl in PBS buffer (pH 4 to 9), data acquired at 20 seconds after addition of HOCl (λ_{ex} = 375 nm).

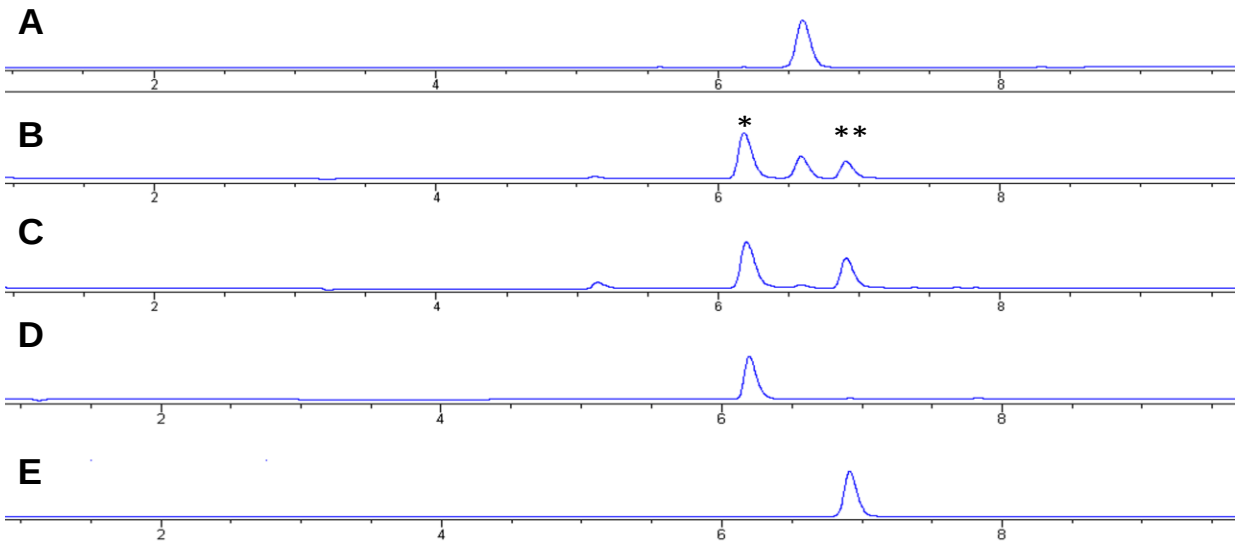

Figure S9. Reversed-phase HPLC chromatograms with absorption (350 nm) detection. The * and ** indicate compound **1** and chlorinated fluorophore (compound **9**), respectively. A) Reversed-phase HPLC chromatograms of 100 μM **TP-HOCl 1**. B) Reversed-phase HPLC chromatograms of 100 μM **TP-HOCl 1** in the presence of 100 μM HOCl for 1 min. C) Reversed-phase HPLC chromatograms of 100 μM probe **TP-HOCl 1** in the presence of 200 μM HOCl for 1 min. D) Reversed-phase HPLC chromatograms of 50 μM compound **1**. E) Reversed-phase HPLC chromatograms of 50 μM chlorinated fluorophore (compound **9**).

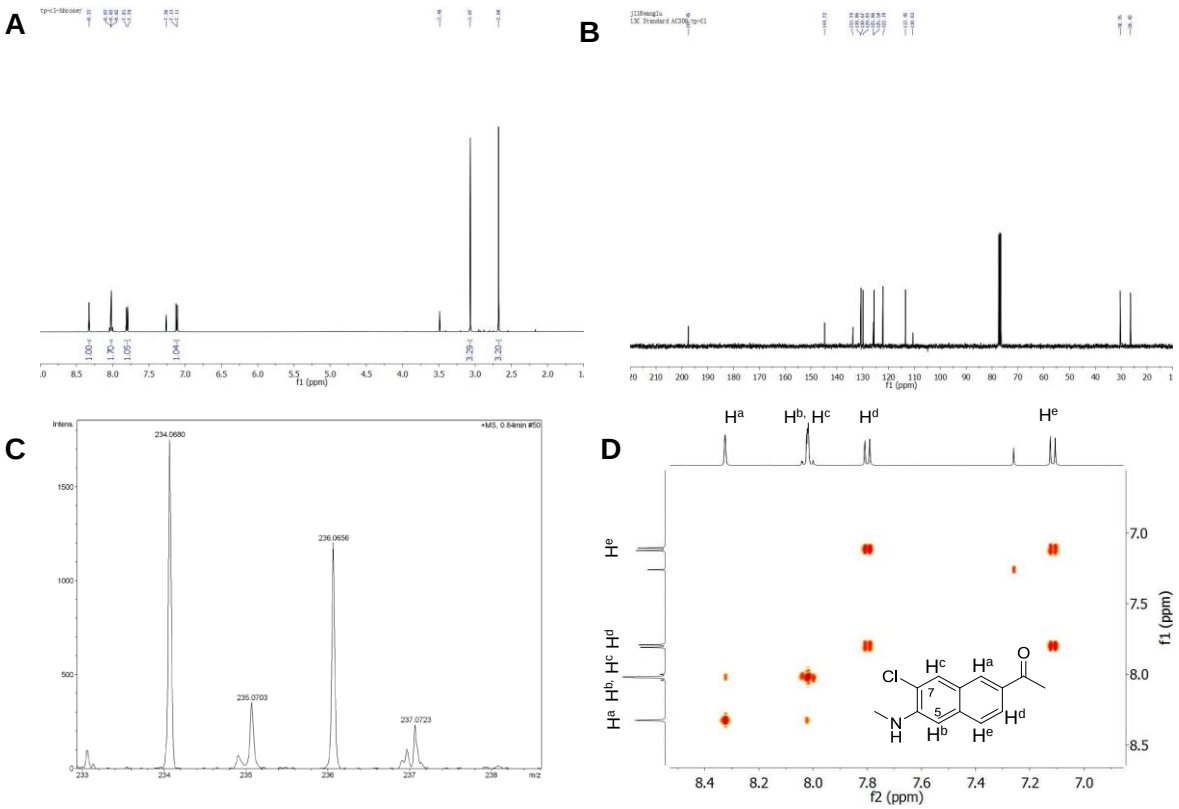

Figure S10. ^{1}H NMR, ^{13}C NMR, HRMS and H-H COSY spectrum of compound **9.** Assignments and proton connectivity of compound **9** were based on vicinal and long-distance *J*-coupling in COSY experiments. All the connections between adjacent protons were observed. The peak at 8.325 ppm was assigned to H^a, which has a long distance *J*-coupling with H^c (δ = 8.023 (d, *J* = 1.5 Hz, 1H). The single peak at 8.018 ppm was assigned to H^b. The correlated proton resonances at 7.800 ppm and 7.115 ppm were assigned to H^d and H^e respectively.

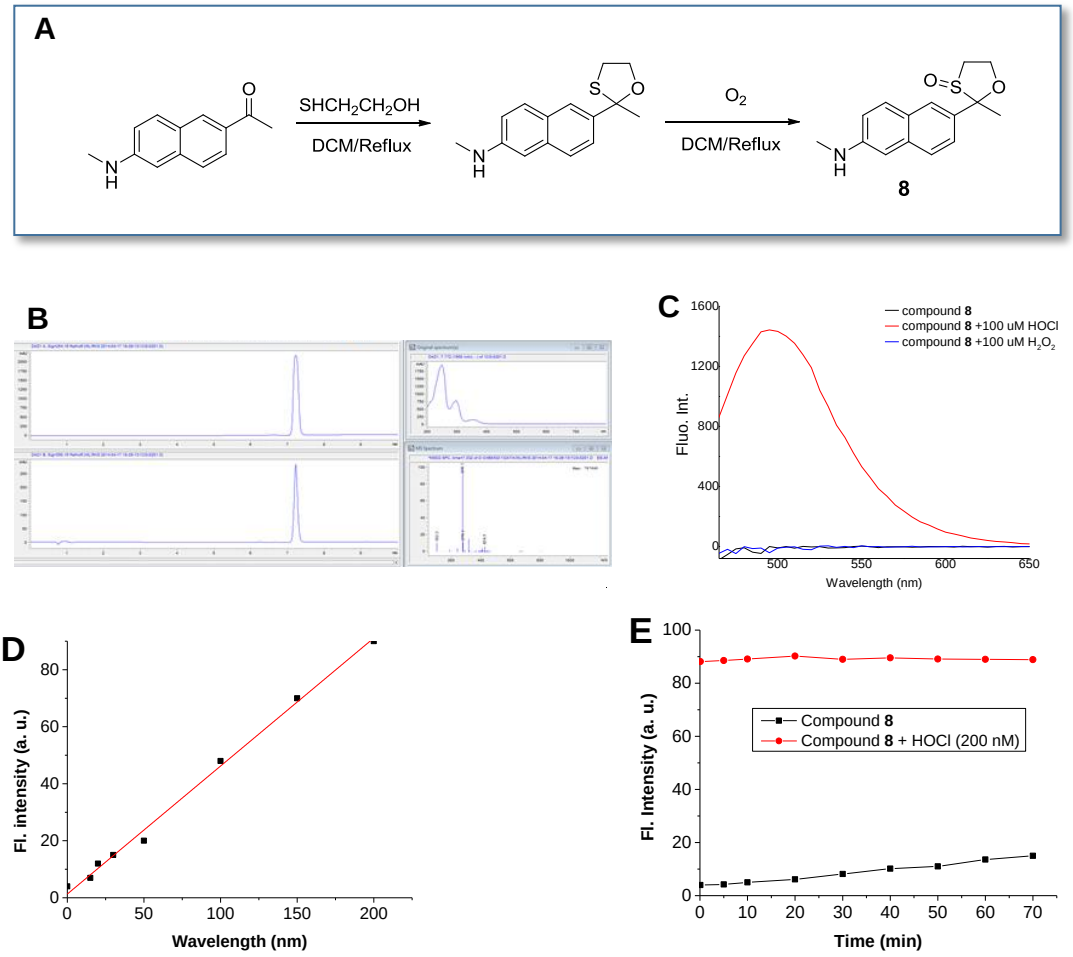

Figure S11. A) Synthetic route toward intermediate **8**. B) The purity and molecular mass of compound **8** was confirmed by Liquid chromatography–mass spectrometry (LC-MS). C) The fluorescence enhancement of compound **8** responding to HOCl rather than H_2O_2 at 100 μM. Probe concentration: 10 μM. Excitation wavelength: 375 nm. D) The fluorescence response of compound **8** to HOCl (15 nM – 200 nM) in PBS/EtOH (1:1, pH 7.4), with the detection limit about 10.3 nM for HOCl. E) Fluorescence intensity of compound **8** and compound **8** in the presence of HOCl (200 nM) with time changes.

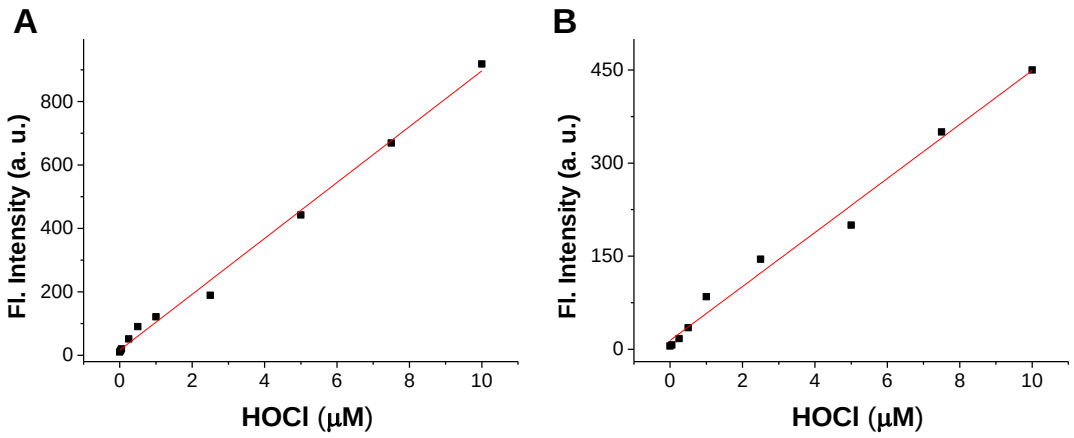

Figure S12. A) The fluorescence response of **MITO-TP** to HOCl (25 nM – 10 μM) in pH 7.4 PBS buffer (1% DMSO). B) The fluorescence respond of **LYSO-TP** to HOCl (50 nM - 10 μM) in pH 5.0 PBS buffer (1% DMSO). Excitation wavelength: 375 nm.

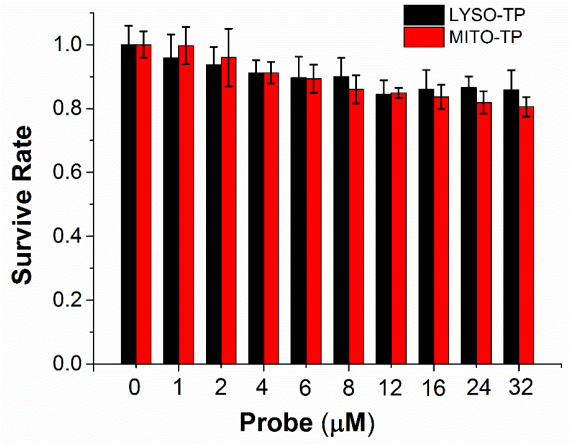

Figure S13. Cytotoxic effect of **MITO-TP** and **LYSO-TP**. HeLa cells were incubated with each concentration of probes for 12 h. Cell viability was assayed with MTT test. Results are expressed as mean ± standard deviation of 5 independent experiments.

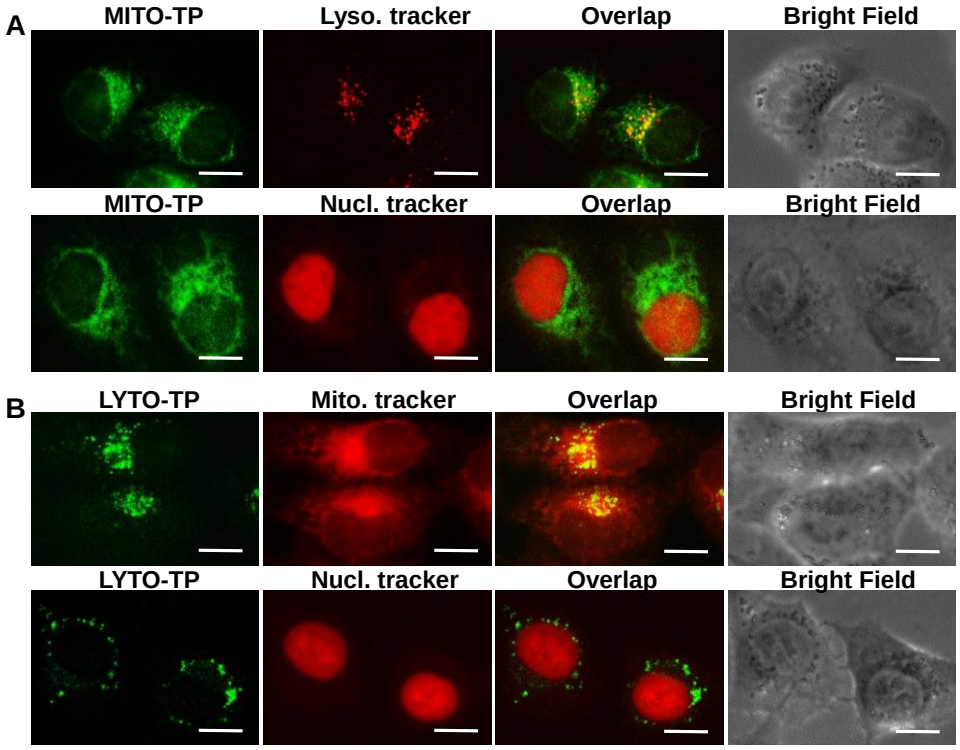

Figure S14. Intracellular localization of **MITO-TP** (A) and **LYSO-TP** (B) in HeLa cells. A) Images of HeLa cells pre-treated respectively with 10 μM **MITO-TP** for 20 min and subsequently 1 μM Lyso-Tracker Red (or 1 μM red cell permeable DNA dye Vybrant® DyeCycle™ Ruby) for 10 min. Then 50 μM HOCl was treated for another 5 min. B) Images of HeLa cells pre-treated respectively with 10 μM **LYSO-TP** for 20 min and subsequently 1 μM Mito-Tracker Red (or 1 μM red cell permeable DNA dye Vybrant® DyeCycle™ Ruby) for 10 min. Then 50 μM HOCl was treated for another 5 min. Green: probe fluorescence; red: Mito-Tracker, Lyso-Tracker and Nucl- Tracker fluorescence (Vybrant® Dye-Cycle™ Ruby); yellow: merged signal. Scale bar: 10 μM.

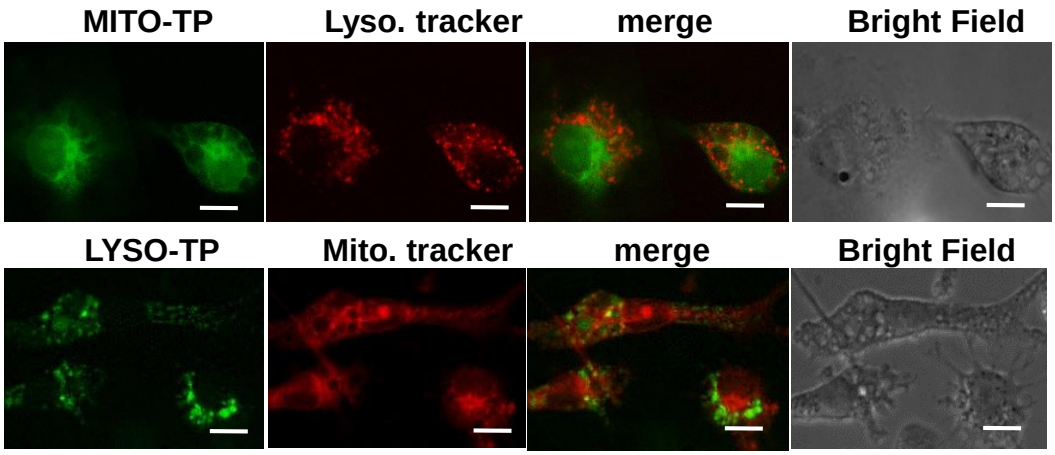

Figure S15. Intracellular distribution of **MITO-TP** and **LYSO-TP** in LPS/IFN-γ-stimulated macrophage cells. RAW 264.7 cells was pre-treated with LPS (120 ng/mL) / IFN-γ (20 ng/mL) for 24 h, then treated with 10 μM **MITO-TP** (or 10 μM **LYSO-TP**) for 20 min and subsequently 1 μM Lyso-Tracker Red (or 1 μM Mito-Tracker Red) for another 10 min. Green: probe fluorescence; red: Mito-Tracker and Lyso-Tracker fluorescence; yellow: merged signal. Scale bar: 10 μM.

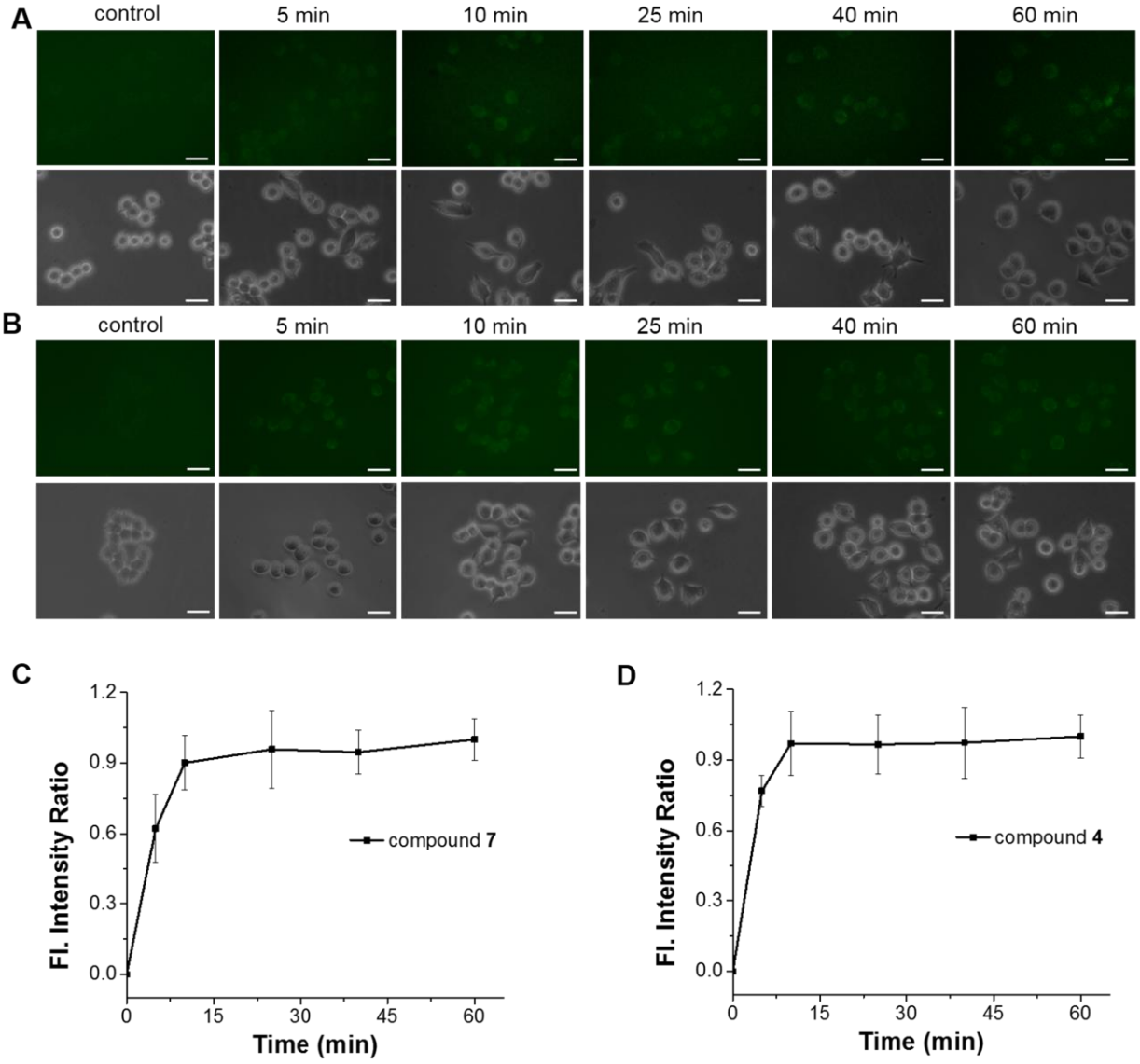

Figure S16. Fluorescent imaging of RAW cells incubated with compound **7** and **4** (precursor of **MITO-TP** and **LYSO-TP**) for different times. A) Compound **7** (10 μM) was incubated with Raw cells for different times and washed by pH 7.4 PBS prior to image. B) Compound **4** (10 μM) was incubated with Raw cells for different times and washed by pH 7.4 PBS prior to image. C, D). Time course of fluorescent intensity ratio of RAW cells after incubation with compound **7** and **4**. The intensities were normalized to that at 60 min. Bright field images were shown below. Error bars are ± SD. n = 3. Scale bar: 30 μM.

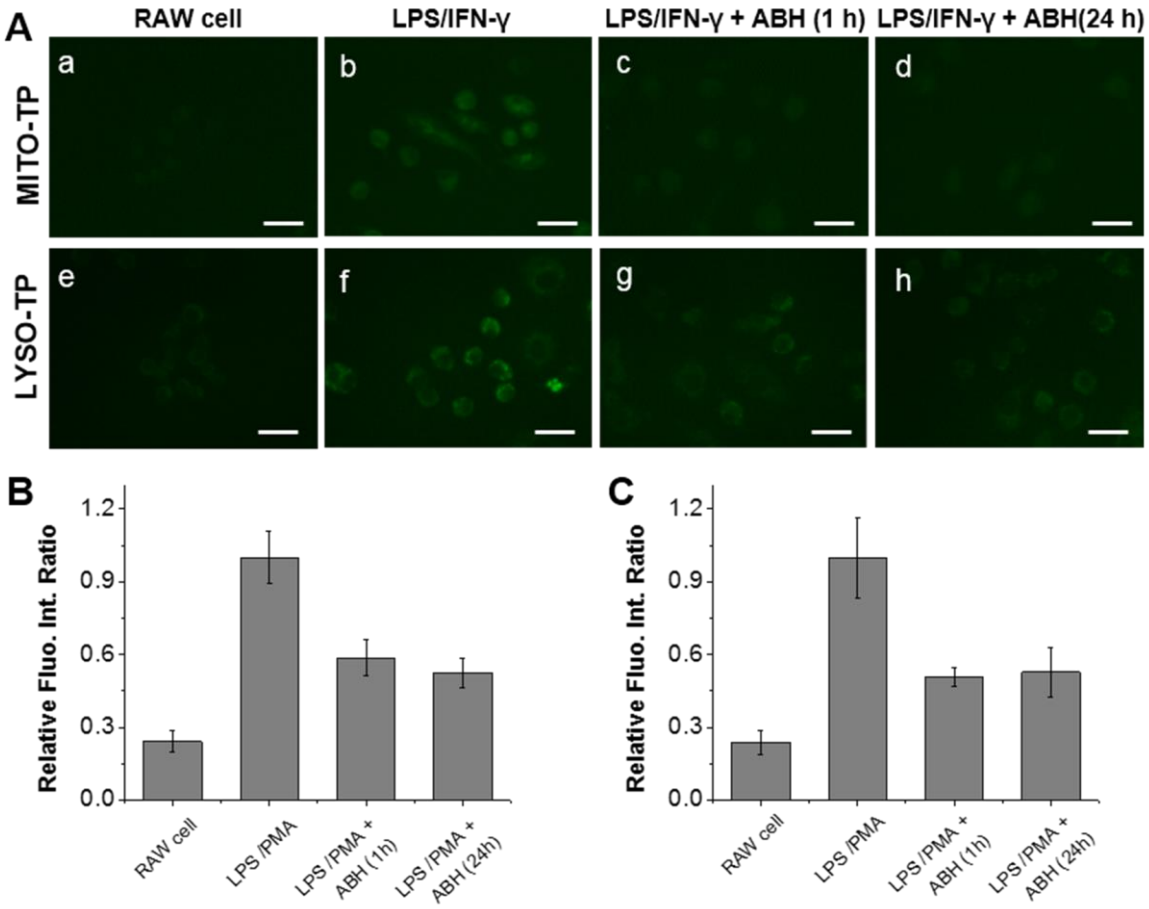

Figure S17. Detection of endogenous HOCl in live RAW 264.7 macrophage cells via **MITO-TP** and **LYSO-TP**. A) Representative fluorescent images of macrophage cells. a, e) **MITO-TP** or **LYSO-TP** (10 μM) was incubated with macrophages cells for 30 min. b, f) Cells were stimulated with LPS (120 ng/mL) / IFN-γ (20 ng/mL) for 24 h and then incubated with **MITO-TP** or **LYSO-TP** (10 μM) for 30 min, washed by PBS buffer prior to imaging. c, g) Cells were stimulated with LPS (120 ng/mL) / IFN-γ (20 ng/mL) for 24 h and then treated with 200 μM ABH for 1 h, subsequently incubated with **MITO-TP** or **LYSO-TP** (10 μM) for 30 min, washed by PBS buffer prior to imaging. d, h) Cells were stimulated with LPS (120 ng/mL) / IFN-γ (20 ng/mL) and ABH (200 μM) for 24 h, subsequently incubated with **MITO-TP** or **LYSO-TP** (10 μM) for 30 min, washed by PBS buffer prior to imaging. B, C) Quantification of the fluorescence signals from a-h. Data were normalized to the fluorescence intensity from LPS/IFN-γ stimulated macrophage cells (b or f). Error bars are ± SD. n = 3. Scale bar: 30 μm.

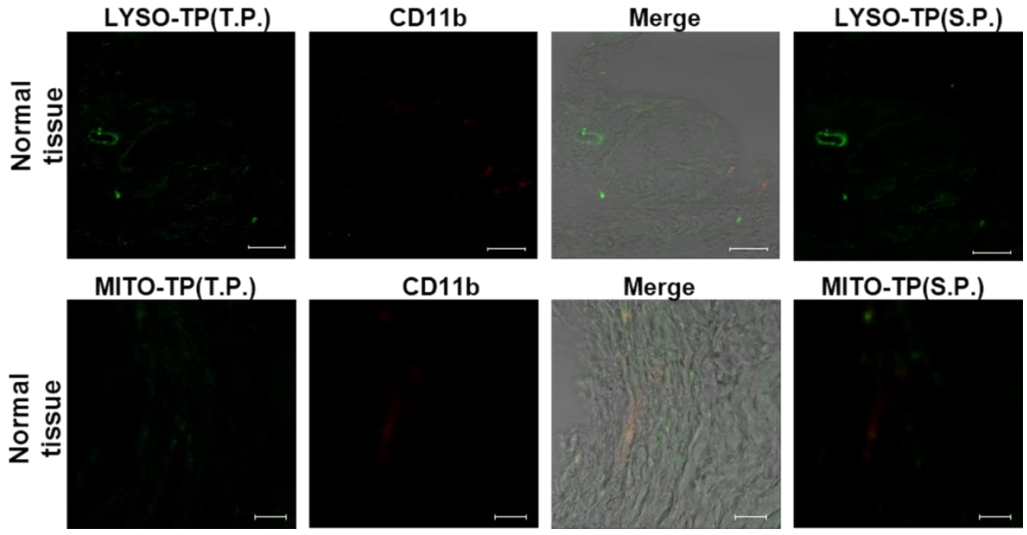

Figure S18. Normal tissue imaging with **LYSO-TP** (or **MITO-TP**) and antibody CD11b. Probe fluorescence was shown in green, antibody CD11b fluorescence was shown in red. Scale bar: 30 μM.

2. Materials and General Experimental Methods

All chemical reagents for the probe synthesis were obtained from Sigma Aldrich, Alfa Aesar, MERCK or Acros, and used without further purification unless otherwise specified. Column chromatography was carried out on Merck Silica Gel 60 (0.040-0.064 mm, 230–400 mesh). Synthetic reactions and analytical characterization were monitored by HPLC-MS (Agilient-1200 series) with a DAD detector and a single quadrupole mass spectrometer (6130 series) with an ESI probe. NMR spectra (^{1}H-300 or 500 MHz and ^{13}C-75 or 125 MHz) were recorded on Bruker Avance 300 or 500 NMR spectrometers. The high resolution electron spray ionization (HR-ESI) mass spectra were obtained on a Bruker micrOTO-FQII. Spectroscopic and quantum yield data were measured on spectroscopic measurements, performed on a fluorometer and UV/VIS instrument, Spectra Max M2 by Molecular Device (The slit width: 1 nm). pH Value was determined by a Mettler Toledo S220 SEVENCOMPACT pH meter (Columbus, OH). Fluorescence microscopic images were obtained from a fluorescence Ti microscope (Nikon) inverted microscope with epifluorescence and phase contrast optics using 20× objective lenses. The green fluorescence was collected by using an Ex 370 nm/40, Em 500 nm/40 filter. Two-Photon tissue images were acquired in Leica TCS SP5 X Confocal Microscope.

3. Synthesis and Characterization

Preparation of TP-HOCl 1, **TP-HOCl 2** and **TP-HOCl 3**. Compound **1** (10 mg, 0.05 mmol), methanesulfonic acid (20 μL) and 2-mercaptoethanol (5.2 mg, 0.06 mmol) (or Ethanedithiol (4.7 mg, 0.06 mmol) or hydroxylamine (4.2 mg, 0.06 mmol)) were mixed in 3 mL dichloromethane solution and refluxed for 3 h under nitrogen protection. The reaction was monitored by HPLC-MS and a product with reduced polarity was observed. Then the mixture was purified by preparative TLC with a solvent system (CH_2Cl_2: hexane = 1:1). Light yellow solid product was obtained.

TP-HOCl 1. Yield: 7.7 mg (59.6%). ^{1}H NMR (300 MHz, CD_2Cl_2) δ 7.82 (d, J = 1.7 Hz, 1H), 7.66 (d, J = 3.1 Hz, 1H), 7.63 (d, J = 2.9 Hz, 1H), 7.50 (dd, J = 8.6, 1.9 Hz, 1H), 6.93 (dd, J = 8.8, 2.4 Hz, 1H), 6.82 (d, J = 2.2 Hz, 1H), 4.40 (ddd, J = 9.1, 6.3, 5.0 Hz, 1H), 4.21 – 4.09 (m, 1H), 3.28 (dt, J = 10.0, 6.6 Hz, 1H), 3.20 – 3.09 (m, 1H), 2.95 (s, 3H), 2.00 (s, 3H). ^{13}C NMR (75 MHz, CD_2Cl_2) δ 147.21, 139.75, 134.38, 128.86, 126.51, 125.78, 124.28, 122.76, 118.02, 103.21, 95.64, 70.73, 34.39, 31.74, 30.44. ESI-MS $C_{15}H_{18}NOS^+$ [M + H^+], found 260.1109, calculated 260.1104.

TP-HOCl 2. Yield: 7.1 mg (51.4 %). ^{1}H NMR (300 MHz, CD_2Cl_2) δ 8.00 (d, J = 2.0 Hz, 1H), 7.85 – 7.73 (m, 1H), 7.64 (dd, J = 8.7, 5.2 Hz, 2H), 6.93 (dd, J = 8.8, 2.4 Hz, 1H), 6.81 (d, J = 2.2 Hz, 1H), 3.63 – 3.37 (m, 4H), 2.96 (d, J = 4.6 Hz, 3H), 2.28 (d, J = 4.5 Hz, 3H). ^{13}C NMR (75 MHz, CD_2Cl_2) δ 147.45, 138.43, 134.19, 128.89, 126.44, 126.17, 125.64, 124.46, 117.92, 103.12, 68.47, 40.50, 33.33, 30.41. ESI-MS: $C_{15}H_{18}NS_2^+$ [M+H^+], found 276.0882, calculated 276.0875.

Preparation of compound 3. Compound **3** was synthesized according the literature procedure.[25]

Preparation of compound 4. Compound **3** (186.1 mg, 1.0 mmol), 2-morpholinoethanamine (65.1 mg, 5.0 mmol) and $Na_2S_2O_5$ (380.2 mg, 2.0 mmol) were dissolved in 4 mL water and stirred at 160 ˚C under microwave (80 mW) for 5 h. After reaction, the solvent was removed under vacuum. The solid product was purified by column chromatography using EtOAc : hexane (1 : 1) solution. Yield: 172 mg, 57.7%. ^{1}H NMR (300 MHz, $CDCl_3$) δ 8.34 (s, 1H), 7.96 (dd, J = 8.6, 1.6 Hz, 1H), 7.77 (d, J = 8.8 Hz, 1H), 7.65 (d, J = 8.7 Hz, 1H), 7.01 (dd, J = 8.8, 2.1 Hz, 1H), 6.81 (d, J = 2.0 Hz, 1H), 3.86 – 3.74 (m, 4H), 3.35 (t, J = 5.8 Hz, 2H), 2.80 – 2.73 (m, 2H), 2.70 (s, 3H), 2.58 (d, J = 4.1 Hz, 4H). ^{13}C NMR (75 MHz, $CDCl_3$) δ 197.94, 148.38, 138.19, 130.97, 130.91, 130.53, 126.08, 126.05, 124.92, 118.82, 103.72, 66.99, 56.85, 53.39, 39.50, 26.57. ESI-MS: $C_{18}H_{23}N_2O_2^+$ [M+H^+], found 299.1765, calculated 299.1754.

Preparation of compound 5. The mixture of compound **3 (**71.0 mg, 0.35 mmol), propane-1,3-diamine (77.5 mg, 1.05 mmol) and $Na_2S_2O_5$ (136.1 mg, 0.70 mmol) in 4.0 mL water and was stirred at 160 ˚C under microwave (80 mW) for 5 h. Then the solvent was removed under vacuum and the solid product was purified by preparative HPLC (method: 0 min, 5 % CH_3CN 7 min, 35% CH_3CN; 9 min 95% CH_3CN; 10 min 5% CH_3CN). The water and acetonitrite mixture was removed under vacuum. Yield: 49.7 mg (53.8%). ^{1}H NMR (500 MHz, DMSO) δ 8.46 (s, 1H), 8.35 (s, 1H), 7.78 (t, J = 9.1 Hz, 2H), 7.58 (d, J = 8.6 Hz, 1H), 7.03 (d, J = 8.8 Hz, 1H), 6.76 (s, 1H), 3.23 (t, J = 6.6 Hz, 2H), 2.90 (t, J = 7.2 Hz, 2H), 2.58 (s, 3H), 1.96 – 1.77 (m, 2H). ^{13}C NMR (75 MHz, DMSO) δ 198.21, 149.69, 138.93, 131.30, 131.25, 130.82, 126.23, 126.15, 124.88, 119.53, 102.93, 37.93, 27.29, 26.40. ESI-MS: $C_{15}H_{19}N_2O^+$ [M+H$^+$], found 243.1496, calculated 243.1492.

Preparation of compound 7. Compound **5** (121.2 mg, 0.50 mmol), Triethylamine (5 μL) and 2-bromoacetyl chloride (86.4 mg, 0.55 mmol) were dissolved in 6 mL dichloromethane and stirred at room temperature for 50 min. The compound **6** was obtained and used to next step without purification. Then 393 mg triphenylphosphine (1.5 mmol) was added into the mixture and stirred at room temperature for 16 h. The light yellow solid product **7** was obtained after purification by column chromatography with CH_2Cl_2 / MeOH (100 : 8) mixture solution. Yield: 223.4 mg (82%). ^{1}H NMR (300 MHz, $CDCl_3$) δ 9.70 (s, 1H), 8.22 (s, 1H), 7.85 (dd, J = 8.7, 1.8 Hz, 1H), 7.80 – 7.67 (m, 9H), 7.63 – 7.55 (m, 7H), 7.53 (d, J = 8.8 Hz, 1H), 7.03 (dd, J = 8.8, 2.2 Hz, 1H), 6.65 (d, J = 2.0 Hz, 1H), 4.89 (d, J = 14.2 Hz, 2H), 3.23 (dd, J = 11.9, 5.9 Hz, 2H), 3.15 (t, J = 6.2 Hz, 2H), 2.62 (s, 3H), 1.74 (dt, J = 12.4, 6.3 Hz, 2H). ^{13}C NMR (75 MHz, $CDCl_3$) δ 197.78, 162.35, 162.29, 148.51, 138.13, 134.97, 134.93, 133.97, 133.83, 130.51, 130.39, 130.19, 130.16, 129.98, 125.65, 125.42, 124.45, 119.06, 118.81, 117.64, 102.70, 40.30, 37.42, 27.06, 26.33. ESI-MS: $C_{35}H_{34}N_2O_2P^+$ [M$^+$], found 545.2360, calculated 545.2352.

Preparation of MITO-TP and LYSO-TP. Compound **4** (29.8 mg, 0.1 mmol) (or compound **7** (54.5 mg, 0.1 mmole)), 2-mercaptoethanol (10.4 mg, 0.12 mmol) and methanesulfonic acid (20 μL) were mixed in 4 mL dichloromethane solution and refluxed for 3 h under nitrogen protection. The reaction was monitored by HPLC-MS and the product with reduced polarity was observed. Then the mixture was purified by preparative TLC with a solvent system (CH_2Cl_2 / Methanol = 100 : 8). Light yellow product was obtained.

LYSO-TP. Yield: 21.8 mg (61.1%). ^{1}H NMR (300 MHz, $CDCl_3$) δ 7.79 (d, J = 1.7 Hz, 1H), 7.62 (d, J = 9.0 Hz, 1H), 7.57 (d, J = 8.5 Hz, 1H), 7.47 (dd, J = 8.6, 1.9 Hz, 1H), 6.94 (dd, J = 8.7, 2.3 Hz, 1H), 6.78 (d, J = 2.1 Hz, 1H), 4.38 (ddd, J = 9.1, 6.4, 4.7 Hz, 1H), 4.09 (ddd, J = 9.1, 7.3, 6.2 Hz, 1H), 3.81 –

3.71 (m, 4H), 3.33 – 3.27 (m, 2H), 3.27 – 3.20 (m, 1H), 3.14 – 3.06 (m, 1H), 2.77 – 2.68 (m, 2H), 2.59 – 2.49 (m, 4H), 1.98 (s, 3H). ^{13}C NMR (75 MHz, $CDCl_3$) δ 146.17, 139.73, 134.35, 129.15, 126.67, 126.01, 124.31, 122.97, 118.30, 104.15, 95.98, 70.60, 66.75, 56.89, 53.25, 39.76, 34.41, 32.07. ESI-MS: $C_{20}H_{27}N_2O_2S^+$ [M+H$^+$], found 359.1800, calculated 359.1788.

MITO-TP. Yield: 39.4 mg (65.2%). ^{1}H NMR (300 MHz, $CDCl_3$) δ 9.89 (t, J = 5.5 Hz, 1H), 7.81 – 7.66 (m, 10H), 7.58 (ddd, J = 10.8, 5.4, 2.5 Hz, 7H), 7.51 (s, 1H), 7.41 (dd, J = 8.6, 1.9 Hz, 1H), 6.95 (dd, J = 8.8, 2.2 Hz, 1H), 6.68 (d, J = 2.1 Hz, 1H), 4.91 (d, J = 14.2 Hz, 2H), 4.35 (ddd, J = 9.1, 6.4, 4.7 Hz, 1H), 4.06 (ddd, J = 9.1, 7.2, 6.2 Hz, 1H), 3.17 – 3.27 (m, 3H), 3.15 – 3.01 (m, 3H), 1.95 (d, J = 6.8 Hz, 3H), 1.79 – 1.68 (m, 2H). ^{13}C NMR (75 MHz, $CDCl_3$) δ 162.43, 162.36, 146.16, 139.13, 134.92, 134.88, 134.43, 133.99, 133.85, 130.14, 129.97, 128.92, 126.29, 125.89, 124.04, 122.94, 118.92, 118.62, 117.75, 103.62, 96.04, 77.42, 77.00, 76.57, 70.55, 41.35, 40.75, 37.50, 34.36, 32.03, 27.36. ESI-MS: $C_{37}H_{38}N_2O_2PS^+$ [M$^+$], found 605.2393, calculated 605.2386.

Preparation of compound 8. Compound **1** (10 mg, 0.05 mmol), 2-mercaptoethanol (5.2 mg, 0.06 mmol) and methanesulfonic acid (20 μL) were mixed in 3 mL dichloromethane (CH_2Cl_2) solution and refluxed for 8 h in air. The solvent was removed under vacuum and the mixture was purified by preparative TLC with a solvent system (CH_2Cl_2 / hexane = 1 : 1). Light yellow product was obtained. Yield: 6.6 mg, 48.2% ^{1}H NMR (300 MHz, $CDCl_3$) δ 7.96 (t, J = 10.8 Hz, 1H), 7.75 (dd, J = 8.7, 2.1 Hz, 1H), 7.60 (dd, J = 8.7, 3.4 Hz, 2H), 6.88 (dd, J = 8.8, 2.4 Hz, 1H), 6.77 (d, J = 2.2 Hz, 1H), 3.55 – 3.37 (m, 4H), 2.93 (s, 3H), 2.23 (d, J = 5.2 Hz, 3H). ^{13}C NMR (75 MHz, $CDCl_3$) δ 147.25, 138.52, 134.20, 129.09, 126.33, 125.95, 124.58, 117.92, 103.57, 68.80, 40.33, 33.40, 30.71. ESI-MS: $C_{15}H_{18}NO_2S^+$ [M + H$^+$], found 276.1058, calculated 276.1053.

Preparation of compound 9. 20 mg (0.1 mmole) compound **1** was mixed with 100 μL NaOCl (4%, 0.11 mmol) in MeOH / H_2O (1 : 1) solution and stirred at room temperature for 2 h. After reaction, 20 mL ice water was added and extracted with dichloromethane (3 x 40 mL). The organic layer was dried by anhydrous Na_2SO_4 and yellow solid product was obtained, which was purified by preparative TLC with dichloromethane and hexane (2 : 1) mixture solvent. Yield: 19.3 mg, 83%. ^{1}H NMR (500 MHz, CD_2Cl_2) δ 8.325 (s, 1H), 8.023 (d, J = 1.5 Hz, 1H), 8.018 (s, 1H), 7.800 (d, J = 8.9 Hz, 1H), 7.115 (d, J = 8.9 Hz, 1H), 3.07 (s, 3H), 2.68 (s, 3H). ^{13}C NMR (125 MHz, $CDCl_3$) δ 197.45, 144.72, 133.79, 130.86, 130.67, 129.83, 125.86, 125.58, 122.19, 113.45, 110.63, 30.35, 26.42. ESI-MS: $C_{13}H_{13}ClNO^+$ [M + H$^+$], found 234.0680, calculated 234.0680.

4. Photo-spectroscopic Studies

Measurement of photo-physical properties. All absorption and emission spectra were recorded on a Spectra Max M2 by Molecular Device at 25 °C. The slit width of both excitation and emission is 1 nm. Stock solutions of the probes in DMSO (10 mM) were used to prepare the working solutions in PBS (0.1M, pH 7.4) / EtOH (1 : 1) or PBS (1% DMSO, pH 7.4 or 5.0) buffer solution with a final concentration of 5.0 μM. Absorbance and emission spectra were recorded immediately after addition of different concentration of HOCl.

Measurements of two-photon fluorescence spectra. Two-photon fluorescence spectra were measured by using a Ti: sapphire oscillator (Avesta Ti-Sapphire TiF-100M) as the excitation source, which gives output of 750 nm laser pulses with pulse duration of 80 fs and repetition rate of 84.5 MHz. The laser beam was filtered through a 750/10 nm bandpass filter (Semrock LD01-785/10-25) to reduce their interference to the measured emission. The sample was excited by a tightly focused laser beam with fluorescence collected at a 90° angle to minimize the scattering. The emission signal was directed into a CCD (Princeton Instruments, Pixis 100B) coupled monochromator (Acton, Spectra Pro 2300i) with an optical fiber.

In vitro **Myeloperoxidase (MPO)/H_2O_2/Cl^- system.** 1 U/mL MPO (Sigma) was dissolved in PBS (pH=7.4, 37 ˚C) and the probe **TP-HOCl 1** (5 ìM) was further added into the solution. After addition of H_2O_2 (20 μM), the fluorescence intensities were recorded immediately in a Spectra Max M2 micro-plate reader. Besides, in inhibition experiment, 10 μM 4-aminobenzoic acid hydrazide (ABH) was added to inhibit MPO before addition of H_2O_2. Furthermore, ABH (4-Aminobenzoic acid hydrazide, 10 μM) or Cys (cysteine, 200 μM) was added at 1 and 2 min respectively.

5. Analytical HPLC analysis

To examine the sensing mechanism of **TP-HOCl 1** responding to HOCl, high pressure liquid chromatography (HPLC) – Mass spectra (MS) were conducted after the incubation of HOCl at different concentration. The signals were recorded at 350 nm and 500 nm as a function of retention time. H_2O (eluent A) / acetonitrile (eluent B) with a linear gradient elution profile: 0 min, 95% A; 1 min, 95% A; 7 min, 5% A; 8.5 min, 5% A; 9 min, 95% A; 10 min, 95% A was used as the mobile phase. The temperature of the column was maintained at 25 ºC and the flow rate of the mobile phase was 1.0 mL/min.

6. *In Vitro* Fluorescence Microscopic Studies

Cell culture. Murine RAW 264.7 cells lines and HeLa cells lines (American Type Culture collection) were grown as mono-layers in 75-cm^2 flasks containing DMEM (BSF) supplemented with 10% FBS (PAA), 1% penicillin streptomycin glutamine (GIBCO) at 37ºC in a humidified incubator of 5% CO_2. Cells were carefully harvested and split when they reached 80% confluence to maintain exponential growth.

Fluorescence microscopic imaging. To avoid the artifacts that occur during fixation procedures, all the experiments were conducted in live cells. The cell experiment can be divided into four groups. The first group is that RAW 264.7 macrophage cells were incubated with 15 μM **MITO-TP** (or **LYSO-TP**) for 20 min. Then the cells were washed by PBS buffer before imaging. In the second group, RAW 264.7 macrophage cells were incubated with 15 μM **MITO-TP** (or **LYSO-TP**) for 20 min, washed by PBS buffer and subsequently incubated with Lipopolysaccharide (LPS, 1 μg/mL) and Phorbol Myristate Acetate (PMA, 1 μg/mL) for 1 h prior to imaging. In the third and fourth the group RAW 264.7 macrophage cells were incubated with 15 μM **MITO-TP** (or **LYSO-TP**) for 20 min, washed by PBS buffer and subsequently incubated with Lipopolysaccharide (LPS, 1 μg/mL) / Phorbol Myristate Acetate (PMA, 1 μg/mL) and 4-aminobenzoic acid hydrazide (ABH, 200 μM) or N-acetylcysteine (NAC, 2 mM) respectively for 1 h prior to imaging.

Determining the subcellular location of probes. Live RAW 264.7 macrophage cells cultured in 35-mm glass bottom culture dishes were incubated with LPS (120 ng/mL) and IFN –γ (20 ng/mL) for 24 h and 10 μM probes (**MITO-TP** and **LYSO-TP**) was further added. After 20 min treatment at 37 ºC, MitoTracker (1.0 μM) and LysoTracker (1.0 μM) were added for another 10 min. Then the cells were washed by PBS prior to imaging. For further confirming the intracellular co-localization, HeLa cells were used to co-localize with trackers. The cells were treated with probes (10 μM) for 20 min and subsequently with Trackers for 10 min, then with 50 μM HOCl for another 5 min. Then the cells were washed by PBS prior to imaging.

Cell cytotoxicity in MTT assay. Cells were plated in 96-well flat-bottomed plates at 1×10^5 cells per well and allowed to grow 12 h prior to exposure to **MITO-TP** and **LYSO-TP**. Then the MTT reagent was added for 4 h at 37 ^oC and DMSO (100 μL/well) was further incubated with cells for 15 min after removing the medium. The absorbance at 570 nm and 690 nm (background signal) was recorded in a Spectra Max M2 microplate reader. The following formula was used to calculate the viability of cell

growth: Cell viability (%) = (mean of A value of treatment group / mean of A value of control) × 100.

7. Two-photon Tissue Imaging Studies

LPS-induced tissue inflammation. After anesthesia, 100 μL of 1 mg/mL LPS (Sigma) was injected on right paws of mice (6-8 week, C57BL6/J). After 1 day, **MITO-TP** and **LYSO-TP** (200 μL, 1 mM) were injected through tail vein. After 1 h, the skin of the inflamed (right paw) and normal (left paw) tissues were harvested and embedded in tissue-freezing medium (Triangle Biomedical Sciences), frozen and consecutively cryo-sectioned into 10 μm or 300 μm segments.

Immunohistofluorescence. The 10 μm segments were carefully rinsed with PBS and fixed with 4% paraformaldehyde for 20 min at room temperature. Then the tissues were treated with 1% bovine serum albumin in PBS for 1 h. For confirmation of HOCl probes stain pattern, rat anti mouse CD11b antibody (Abcam, dilution factor 1:300) was applied and was visualized by cy5-conjugated goat anti rat secondary antibody (Life Technologies™, dilution factor 1:300). All imagings were taken by Leica TCS SPS X two photon microscope. The excitation wavelength is 750 nm and the collection wavelength range is from 450-520 nm. For the detection of cy5, the excitation wavelength is 630 nm and the collection wavelength range is from 650-670 nm.

Two-photon inflamed tissue imaging. The 300 μm segments were carefully rinsed with PBS and covered with coverslip. Leica TCS SPS X microscope was used to take two photon imaging. The excitation wavelength is 750 nm and the collection wavelength range is from 450-520 nm. 3D construction was performed in Leica TCS SPS X software.

8. Supplemental Spectra

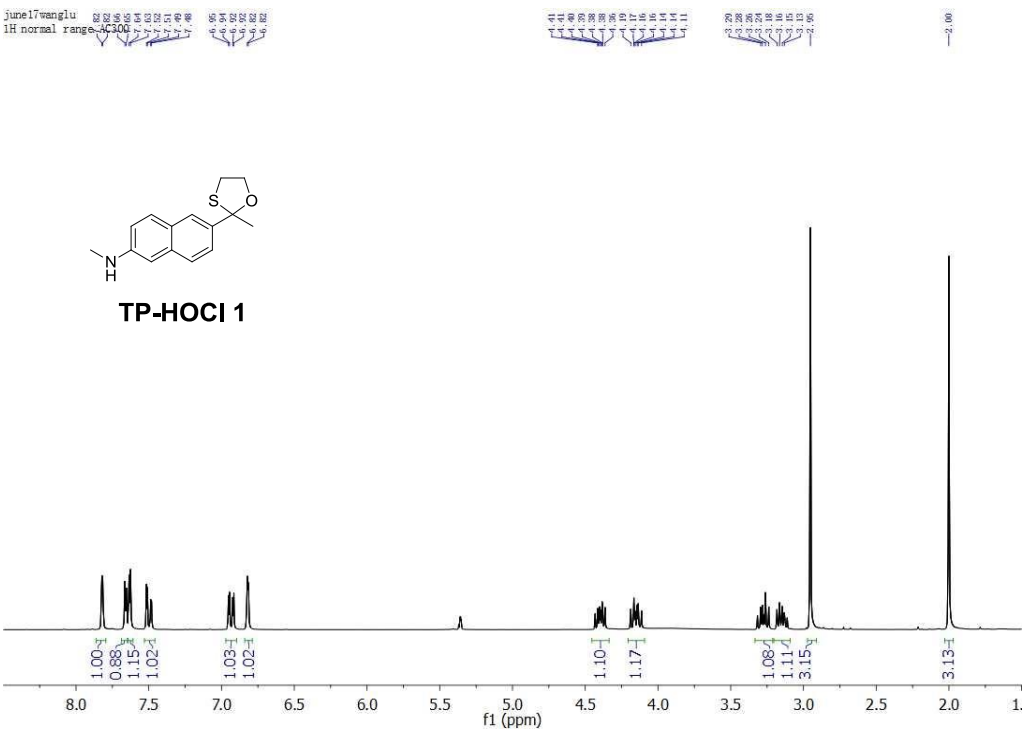

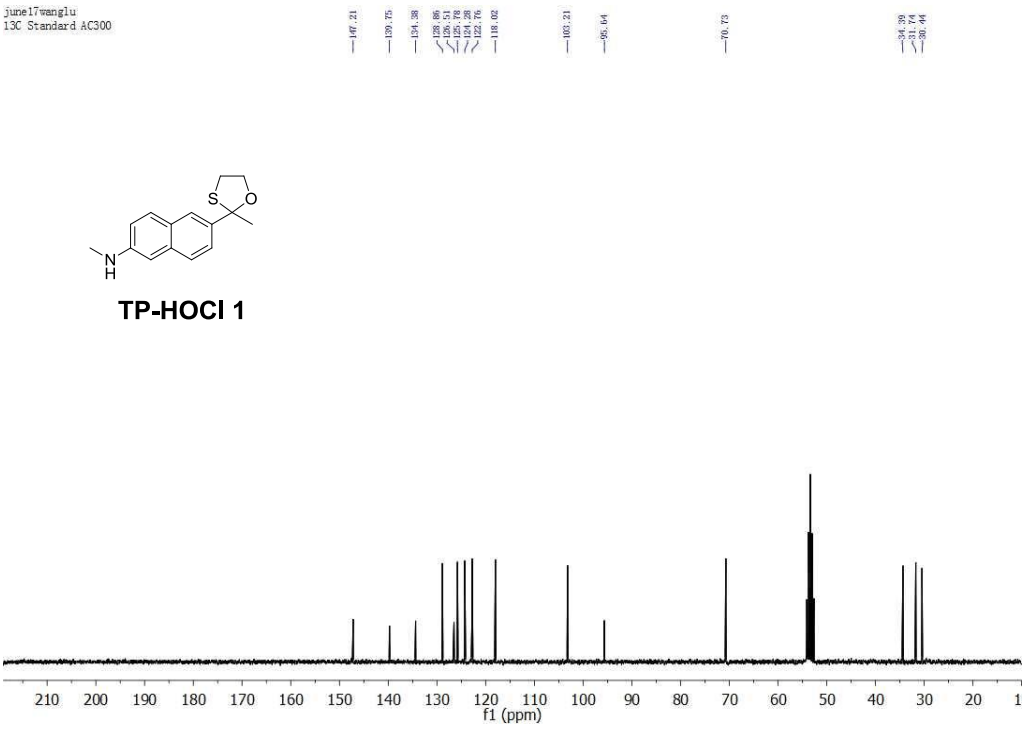

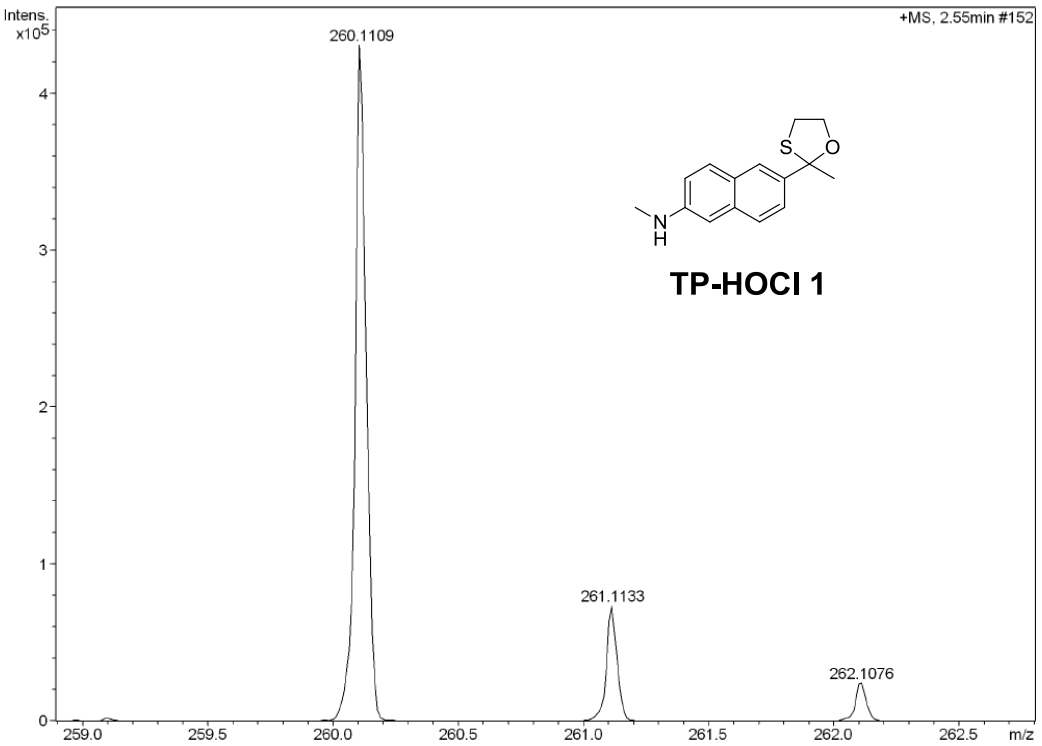

TP-HOCl 1

TP-HOCl 2

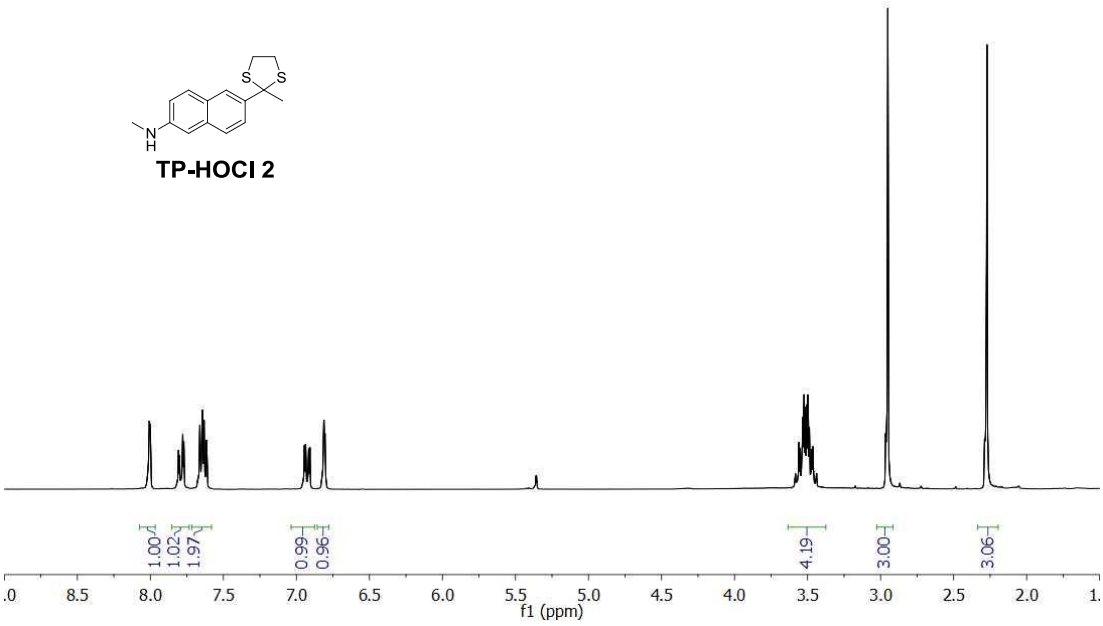

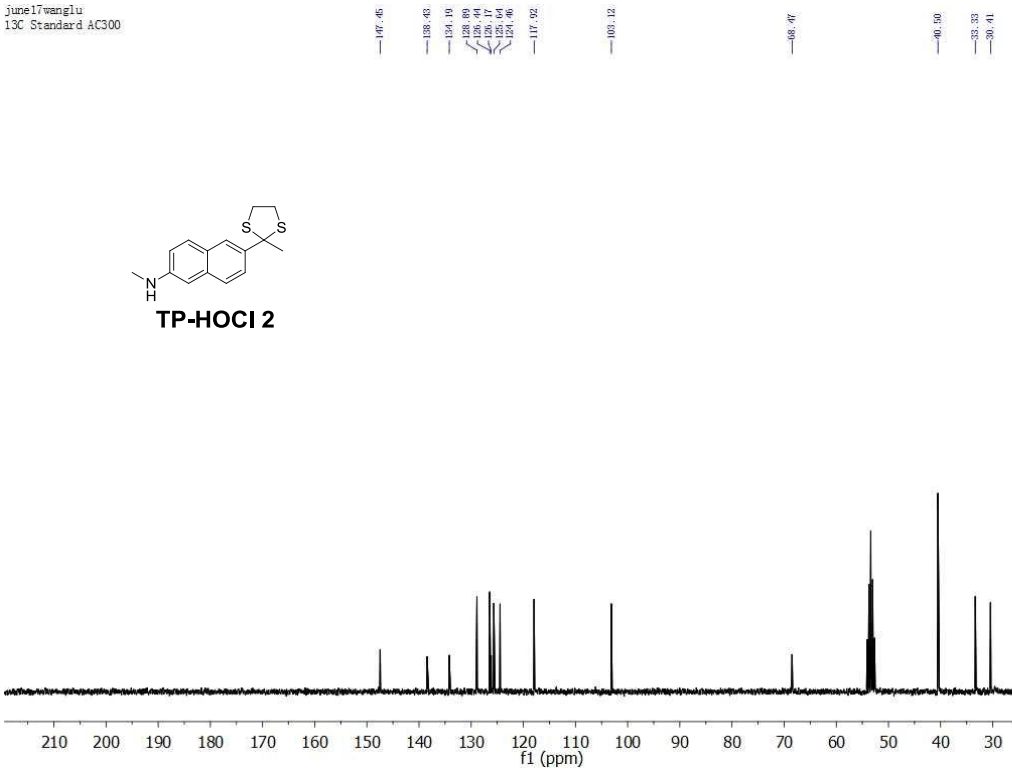
june17wanglu
13C Standard AC300
147.45
138.43
134.19
128.89
126.44
126.17
125.64
124.46
117.92
103.12
68.47
40.50
33.33
30.41
TP-HOCl 2
f1 (ppm)
ju23wanglu
1H normal range AC300
8.30
7.94
7.93
7.91
7.90
7.74
7.71
7.62
7.59
7.26
6.98
6.97
6.95
6.95
6.77
6.77
3.77
3.75
3.74
3.33
3.31
3.29
2.74
2.72
2.70
2.69
2.54
2.53
4
1.02
0.99
1.03
1.00
0.97
0.97
4.16
1.98
2.26
3.03
3.96
f1 (ppm)

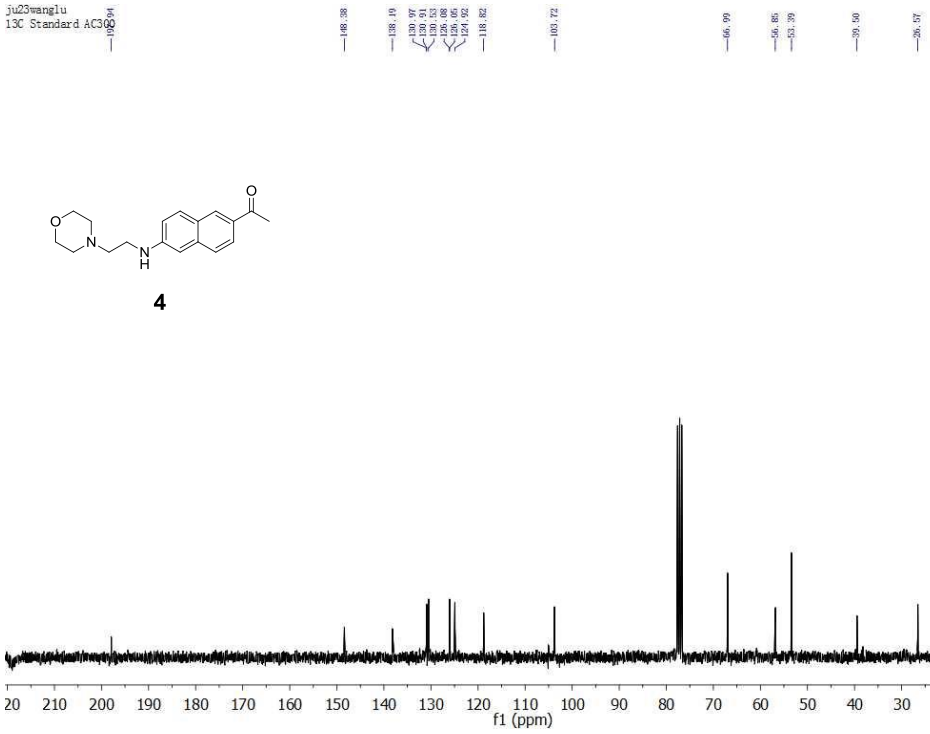
ju23wanglu
13C Standard AC300
197.94
148.38
138.19
130.97
130.91
130.53
126.88
126.05
124.92
118.82
103.72
66.99
56.85
53.39
39.50
26.57
O
O
N
N
H
4
20 210 200 190 180 170 160 150 140 130 120 110 100 90 80 70 60 50 40 30 20 10
f1 (ppm)

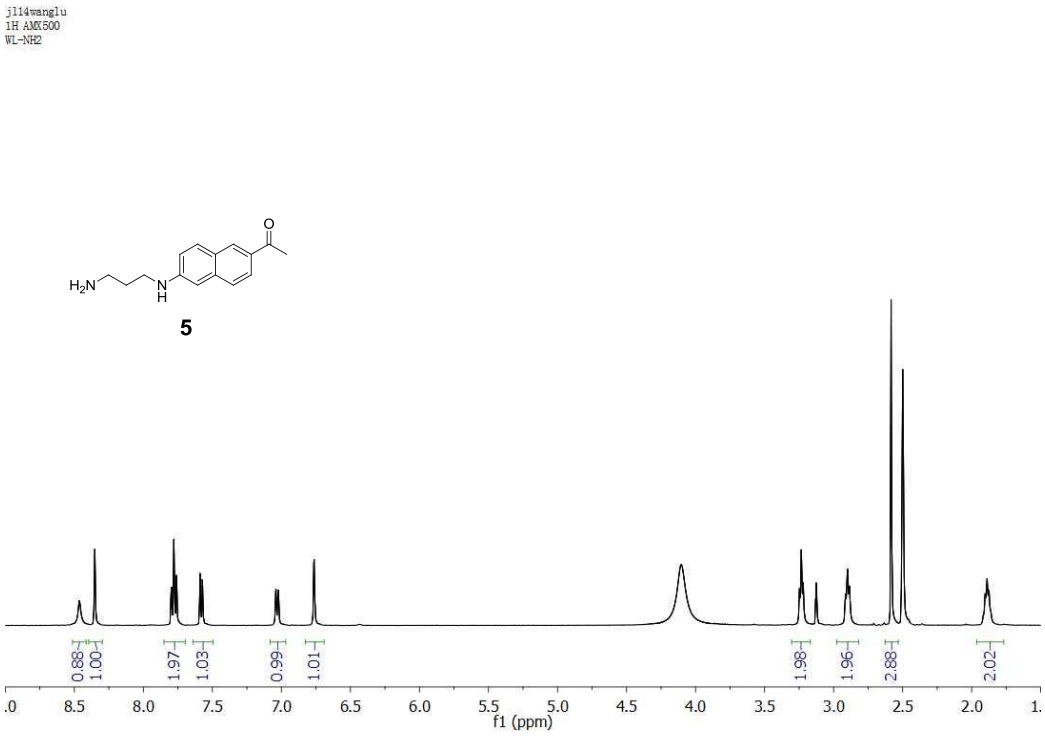
jl14wanglu
1H AMX500
WL-NH2
O
H2N
N
H
5
0.88
1.00
1.97
1.03
0.99
1.01
1.98
1.96
2.88
2.02
.0 8.5 8.0 7.5 7.0 6.5 6.0 5.5 5.0 4.5 4.0 3.5 3.0 2.5 2.0 1.
f1 (ppm)

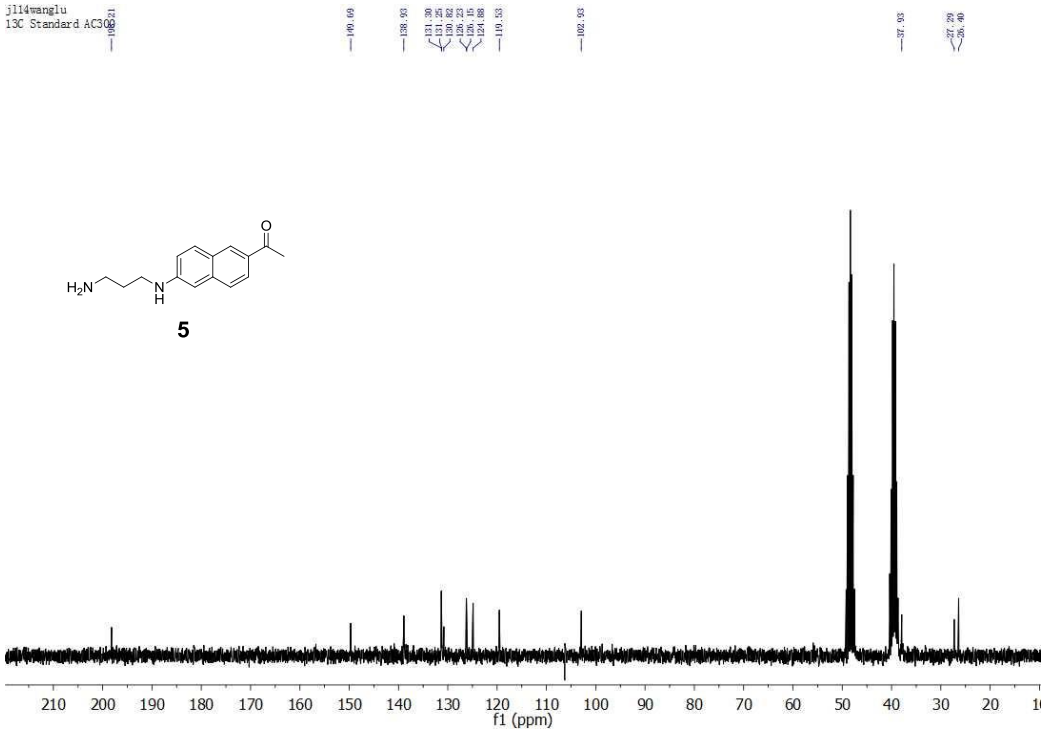
j114wanglu
13C Standard AC300
f1 (ppm)

5

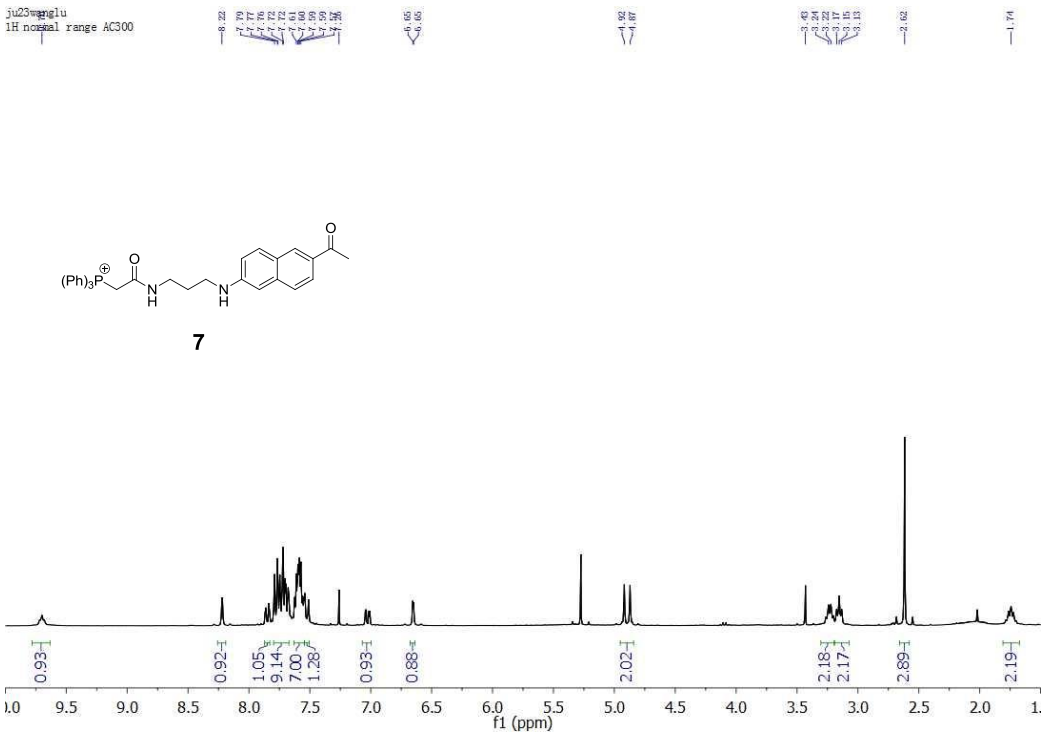
ju23wanglu
1H normal range AC300
0.93
0.92
1.05
9.14
7.00
1.28
0.93
0.88
2.02
2.18
2.17
2.89
2.19
f1 (ppm)

7

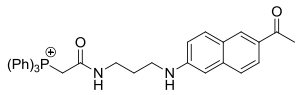

7

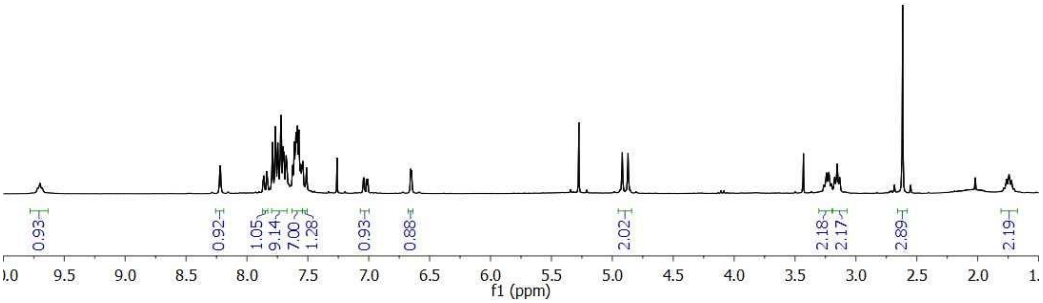
0.93
0.92
1.05
9.14
7.00
1.28
0.93
0.88
2.02
2.18
2.17
2.89
2.19
f1 (ppm)

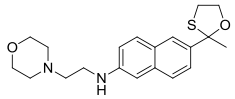

LYSO-TP

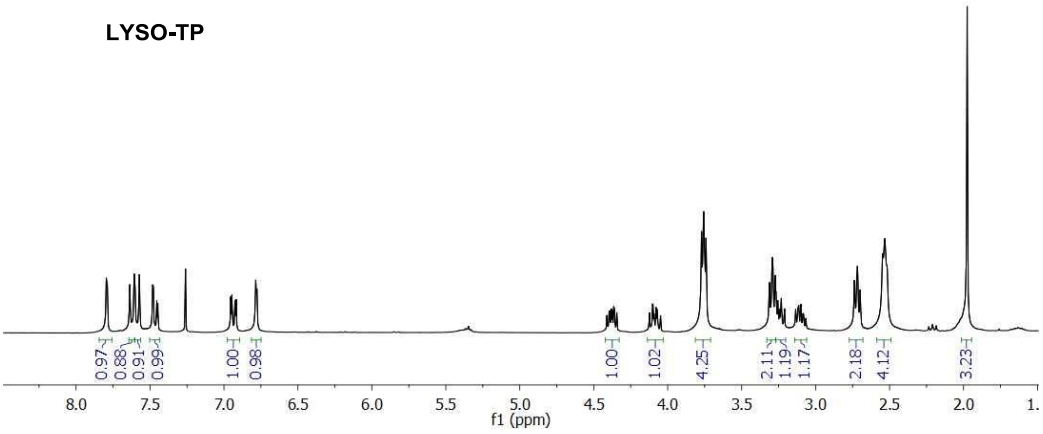
0.97
0.88
0.91
0.99
1.00
0.98
1.00
1.02
4.25
2.11
1.19
1.17
2.18
4.12
3.23
f1 (ppm)

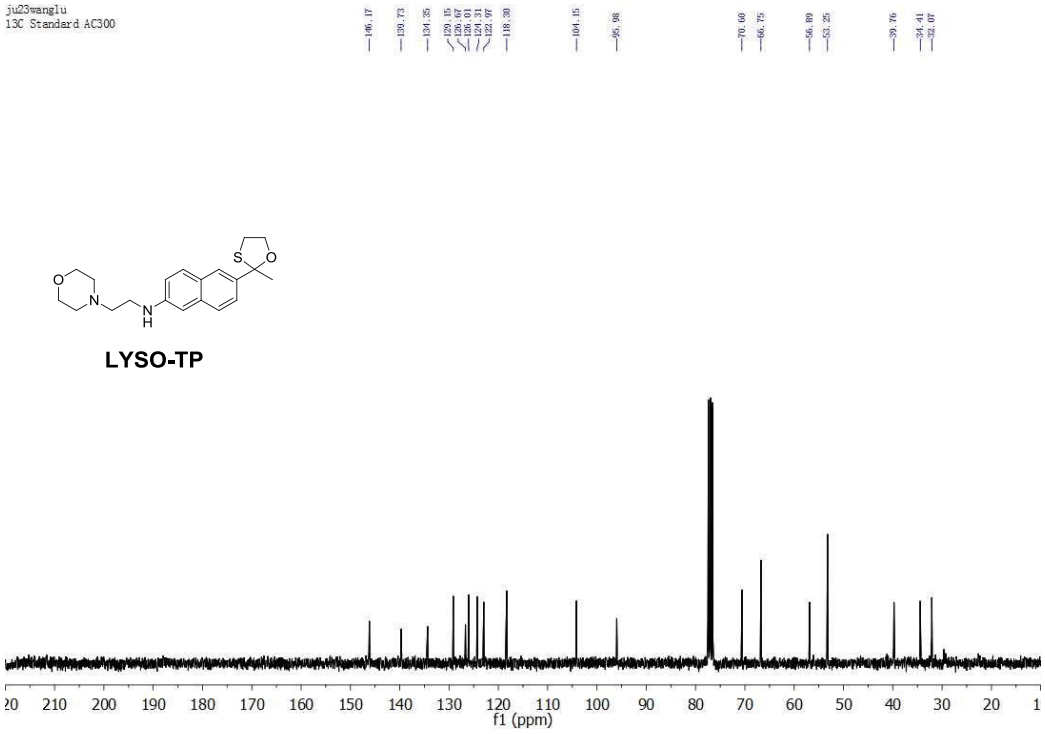
ju23wanglu
13C Standard AC300
146.17
139.73
134.35
129.15
126.67
126.01
124.31
122.97
118.30
104.15
95.98
70.60
66.75
56.89
53.25
39.76
34.41
32.07
LYSO-TP
f1 (ppm)

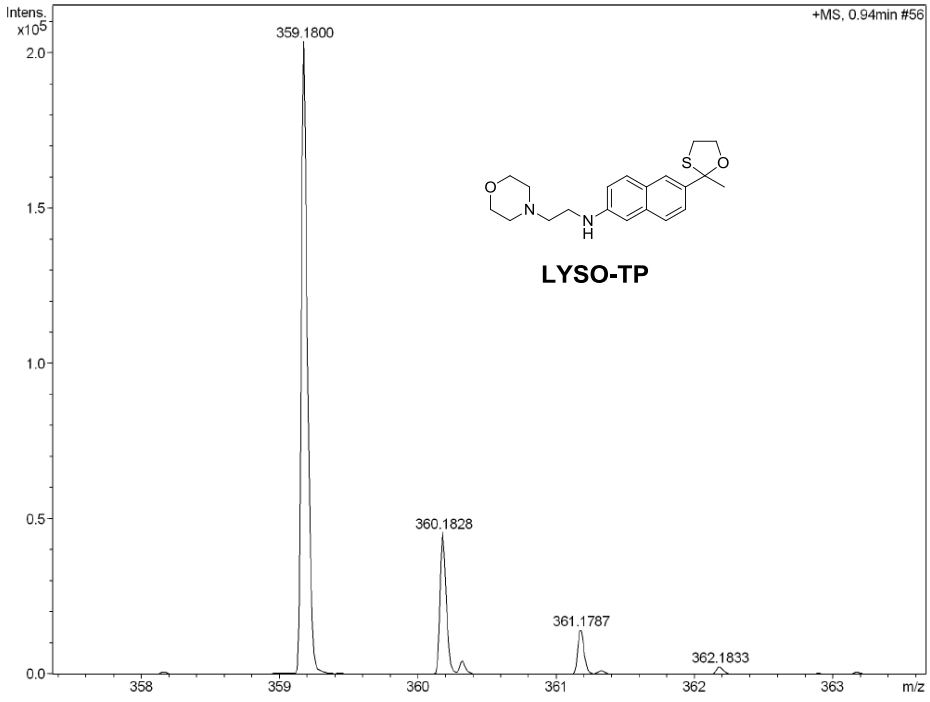
Intens.
x10^5
+MS, 0.94min #56
359.1800
360.1828
361.1787
362.1833
LYSO-TP
m/z

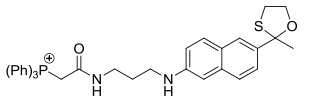

MITO-TP

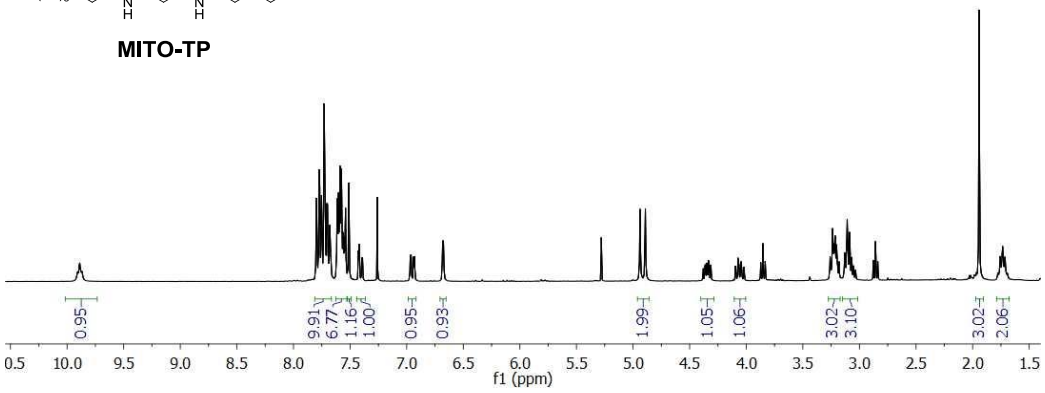

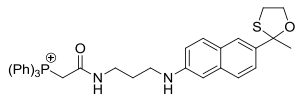

MITO-TP

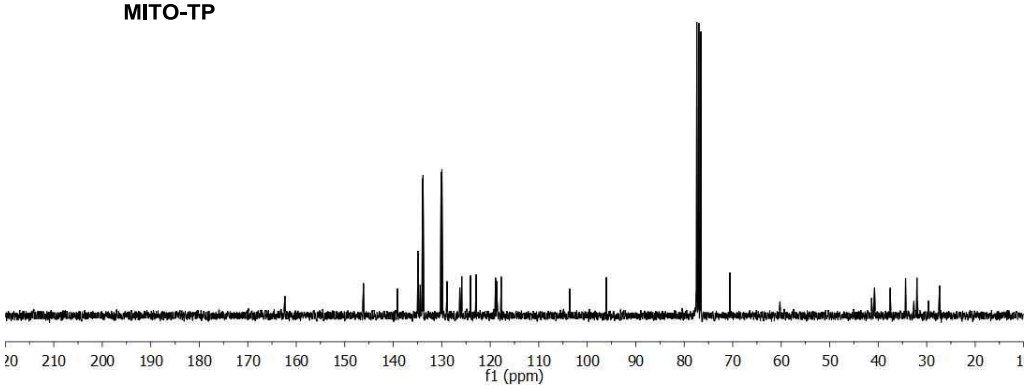

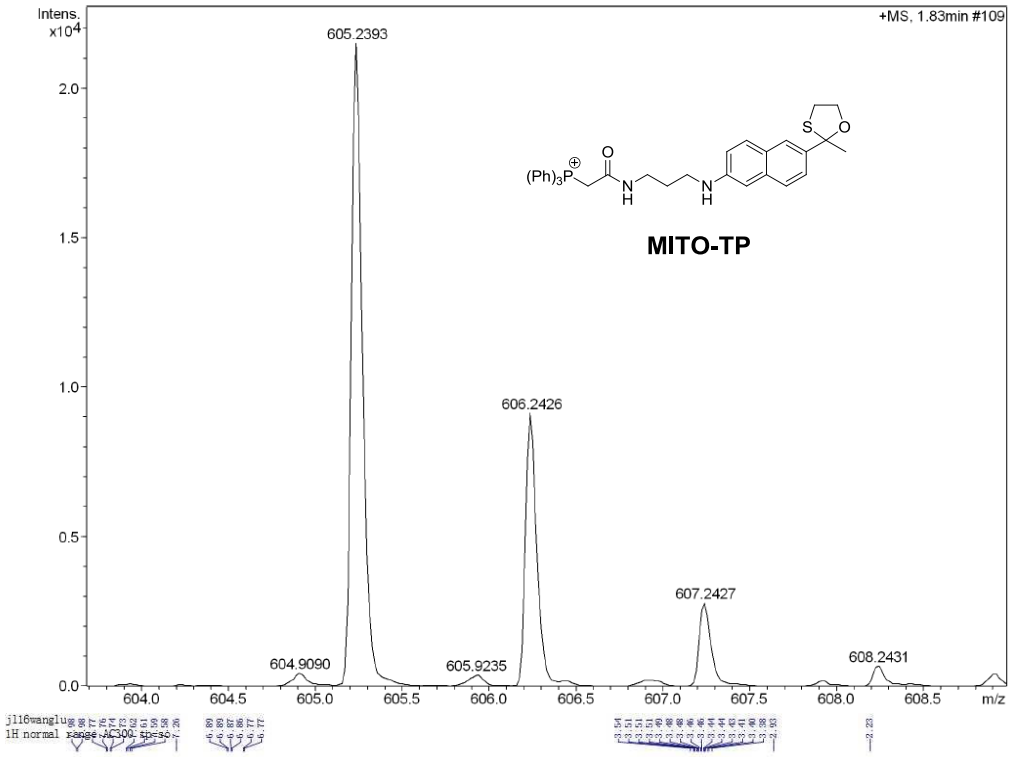
Intens.
x10^4
+MS, 1.83min #109
605.2393
606.2426
607.2427
604.9090
605.9235
608.2431
m/z
MITO-TP

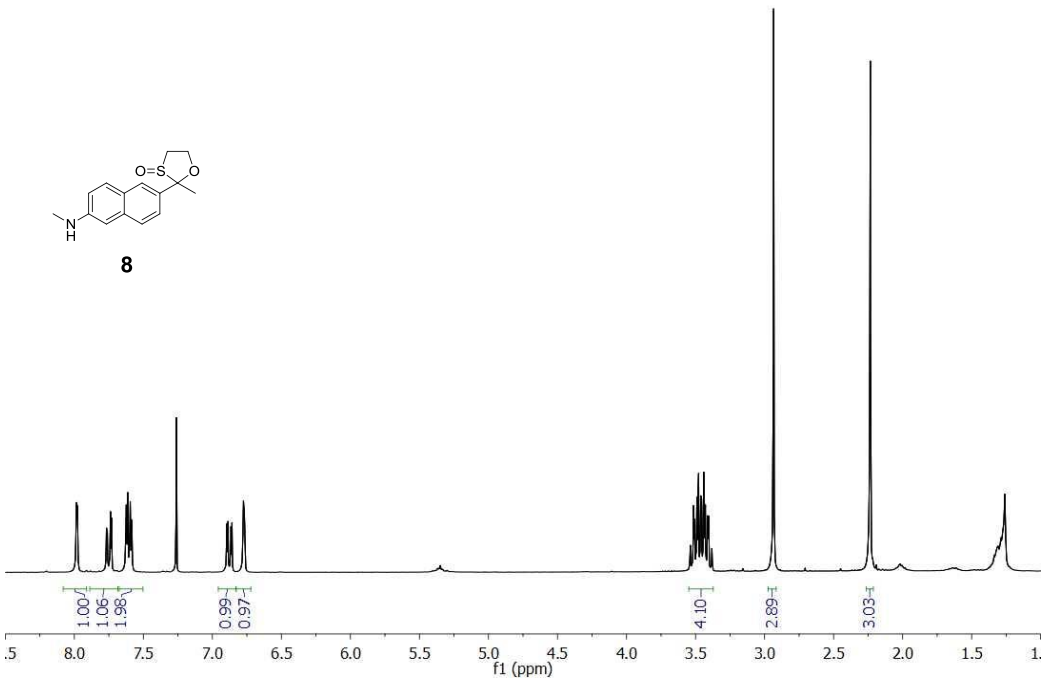
8
1.00
1.06
1.98
0.99
0.97
4.10
2.89
3.03
f1 (ppm)

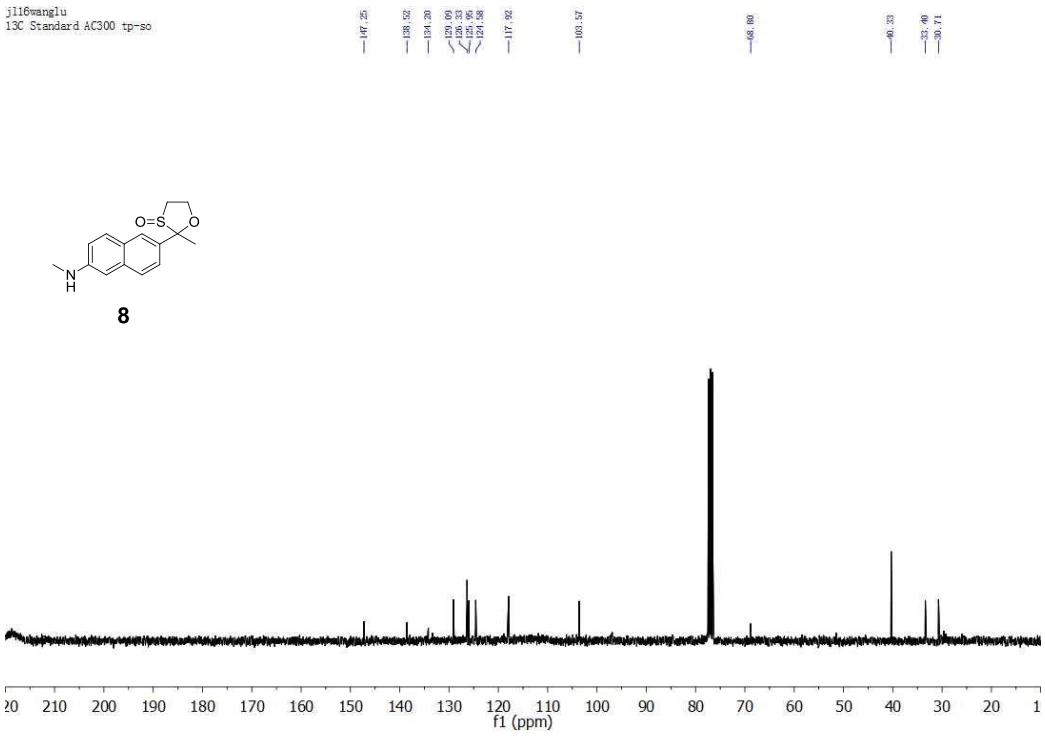

9. Reference:

1. Chen, X.; Wang, X.; Wang, S.; Shi, W.; Wang, K.; Ma, H. *Chem. Eur. J.* **2008**, *14*, 4719.

2. Kenmoku, S.; Urano, Y.; Kojima, H.; Nagano, T . *J. Am. Chem. Soc.* **2007,** *129*, 7313.

3. Koide, Y.; Urano, Y.; Hanaoka, K.; Terai, T.; Nagano, T. *J. Am. Chem. Soc.* **2011**, *133*, 5680.

4. Zhan, X.-Q.; Yan, J.-H.; Su, J.-H.; Wang, Y.-C.; He, J.; Wang, S.-Y.; Zheng, H.; Xu, J.-G. *Sensor. Actuat. B: Chem.* **2010**, *150*, 774.

5. Chen, X.; Lee, K. A.; Ha, E. M.; Lee, K. M.; Seo, Y. Y.; Choi, H. K.; Kim, H. N.; Kim, M. J.; Cho, C. S.; Lee, S. Y.; Lee, W. J.; Yoon, J. *Chem. Commun.* **2011**, *47*, 4373.

6. Xu, Q.; Lee, K. A.; Lee, S.; Lee, K. M.; Lee, W. J.; Yoon, J. *J. Am. Chem. Soc.* **2013**, *135*, 9944.

7. Zhang, R.; Ye, Z.; Song, B.; Dai, Z.; An, X.; Yuan, J. *Inorg. Chem.* **2013**, *52*, 10325.

8. Ye, Z.; Zhang, R.; Song, B.; Dai, Z.; Jin, D.; Goldys, E. M.; Yuan, J. *Dalton Trans.* **2014**, *43*, 8414.

9. Yuan, L.; Lin, W.; Xie, Y.; Chen, B.; Song, J. *Chem. Eur. J.* **2012**, *18*, 2700.

10. Sun, Z. N.; Liu, F. Q.; Chen, Y.; Tam, P. K.; Yang, D. *Org. Lett.* **2008**, *10*, 2171.

11. Hu, J. J.; Wong, N. K.; Gu, Q.; Bai, X.; Ye, S.; Yang, D. *Org. Lett.* **2014**, *16*, 3544.

12. Lin, W.; Long, L.; Chen, B.; Tan, W. *Chem. Eur. J.* **2009**, *15*, 2305.

13. Cheng, X.; Jia, H.; Long, T.; Feng, J.; Qin, J.; Li, Z. *Chem. Commun.* **2011**, *47*, 11978.

14. Emrullahoglu, M.; Ucuncu, M.; Karakus, E. *Chem. Commun.* **2013**, *49*, 7836.

15. Zhao, N.; Wu, Y. H.; Wang, R. M.; Shi, L. X.; Chen, Z. N. *Analyst* **2011**, *136*, 2277.

16. Zhu, H.; Fan, J.; Wang, J.; Mu, H.; Peng, X. *J. Am. Chem. Soc.* **2014**, *136*, 12820.

17. Cheng, G.; Fan, J.; Sun, W.; Cao, J.; Hu, C.; Peng, X. *Chem. Commun.* **2014**, *50*, 1018.

18. Liu, S. R.; Wu, S. P. *Org. Lett.* **2013**, *15*, 878.

19. Li, G.; Zhu, D.; Liu, Q.; Xue, L.; Jiang, H. *Org. Lett.* **2013**, *15*, 2002.

20. Qu, Z.; Ding, J.; Zhao, M.; Li, P. *J. Photoch. Photobio. A* **2015**, *299*, 1.

21. Wu, X. J.; Li, Z.; Yang, L.; Han, J. H.; Han, S. F. *Chem. Sci.* **2013**, *4*, 460.

22. Xiao, H.; Xin, K.; Dou, H.; Yin, G.; Quan, Y.; Wang, R. *Chem. Commun.* **2015**, *51*, 1442.

23. Li, G.; Lin, Q.; Ji, L.; Chao, H. *J. Mater. Chem. B* **2014**, *2*, 7918.

24. Hou, J.-T.; Wu, M.-Y.; Li, K.; Yang, J.; Yu, K.-K.; Xie, Y.-M.; Yu, X.-Q. *Chem. Commun.* **2014,** *50*, 8640.

25. This work.